Advanced Gas Turbine

AGT

Power-Train System Development

DOE/NASA/0168-5
NASA CR-168056
DDA EDR 11185

Fifth Semiannual Report
For work performed from January 1982 - June 1982

Detroit Diesel Allison
Division of General Motors Corporation
Indianapolis, Indiana 46206

August 1982

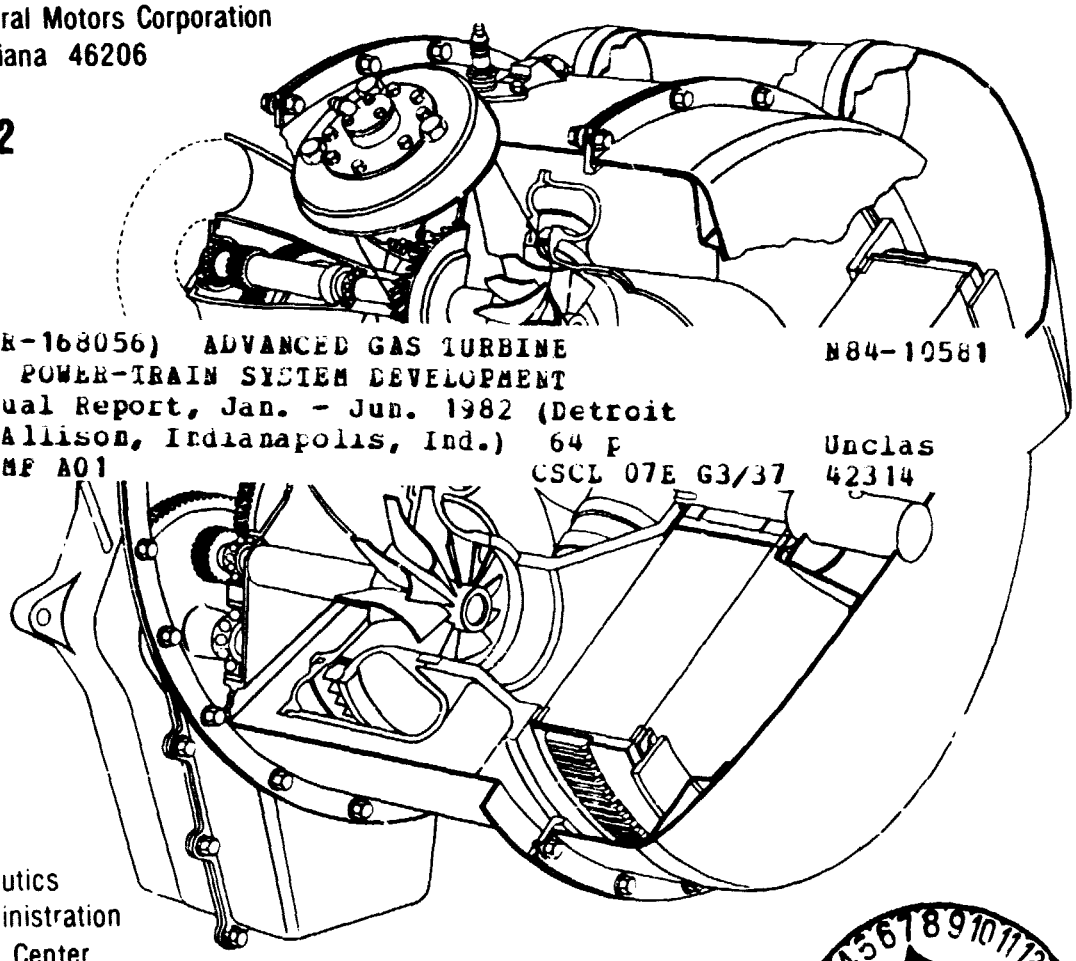

Prepared for
National Aeronautics
and Space Administration
Lewis Research Center
Cleveland, Ohio 44135
Contract DEN 3-168

For U. S. Department of Energy
Conservation and Renewable Energy
Office of Vehicle and Engine Research and Development

NOTICE

DOE/NASA/0168-5
NASA CR-168056
DDA EDR 11185

Advanced Gas Turbine (AGT) Power-Train System Development

Fifth Semiannual Report
For work performed from January 1982-June 1982

H. E. Helms, R. A. Johnson, R. K. Gibson, L. B. Smith
Detroit Diesel Allison
Division of General Motors Corporation

August 1982

Prepared for
NATIONAL AERONAUTICS AND SPACE ADMINISTRATION
Lewis Research Center
Under Contract DEN 3-168

for
U. S. DEPARTMENT OF ENERGY
Conservation and Renewable Energy
Office of Vehicle and Engine Research and Development

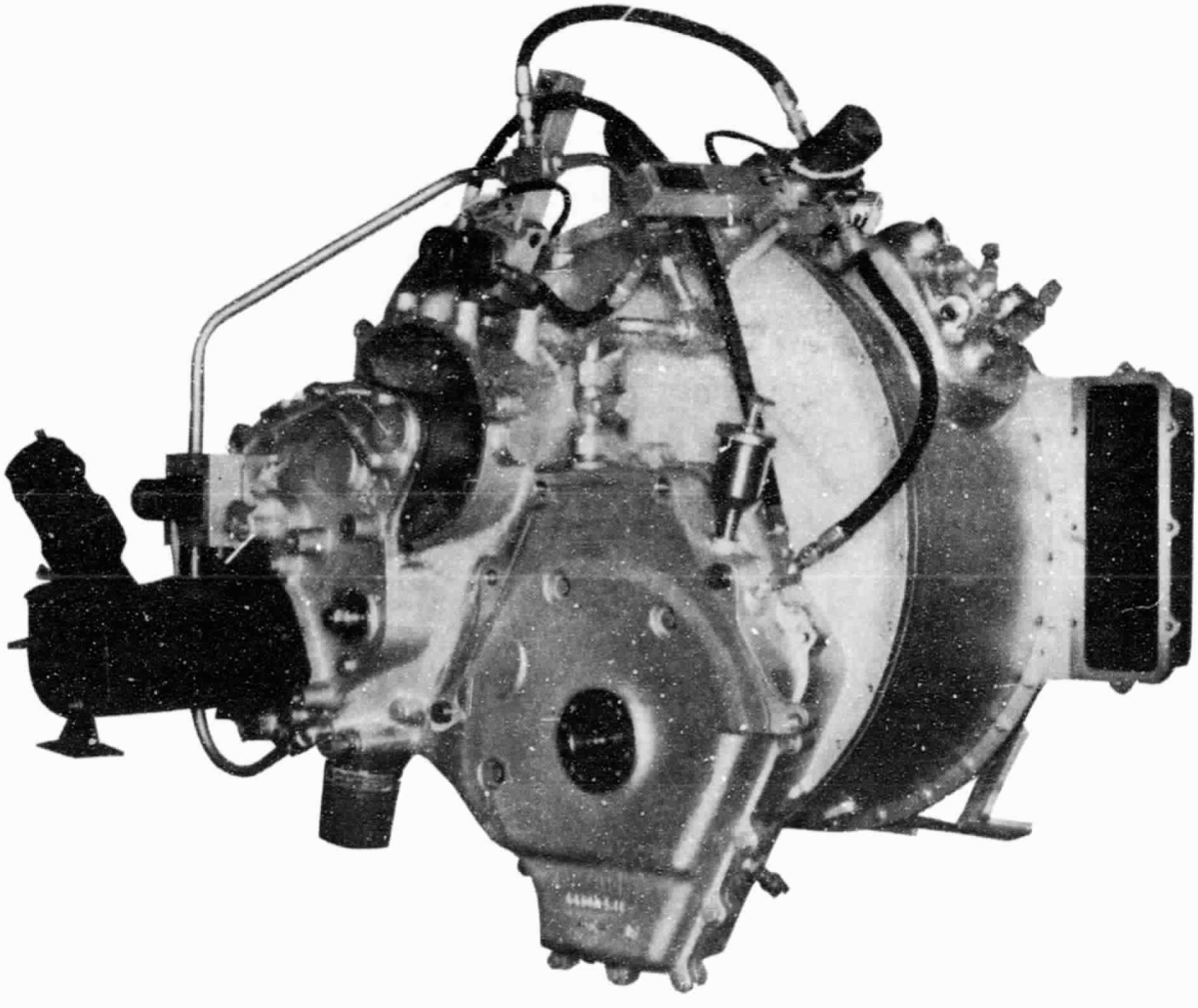

Assembled AGT 100 engine

FOREWORD

This report presents a technical summary of the Detroit Diesel Allison (DDA) project to develop an automotive gas turbine power-train system under NASA Contract DEN3-168 (Department of Energy funding). It covers the 6-month period January through June 1982.

The basic objective of this project is to develop and demonstrate, by May 1985, an advanced automotive gas turbine power-train system that will, when installed in a 1984 Pontiac Phoenix vehicle of 1364 kg (3,000 lb) inertia weight, achieve a fuel economy of 18 km/L (42.5 mpg), meet or exceed the 1985 emission requirements, and have alternate fuel capability.

Several General Motors Divisions and other companies are major contributors to this effort: Pontiac Motor Division – vehicle, Delco Remy Division – starter/boost motor, Harrison Radiator Division and Corning Glass Works – regenerator, and the Carborundum Company and GTE – ceramics.

The DDA Program Manager for the AGT 100 is H. E. (Gene) Helms, design effort is directed by James Williams, materials effort is directed by Dr. Peter Heitman, and project effort is directed by Richard Johnson. The Pontiac effort is headed by Leighton Smith. The NASA AGT 100 Project Manager is Paul T. Kerwin.

TABLE OF CONTENTS

Section	Title	Page
	Summary	1
	Introduction	3
I	Vehicle System Development (vehicle effort deleted)	
II	Engine/Power-Train Development	5
	2.2 Mod I	5
	Engine Build	5
	Performance	6
III	Compressor Development	7
	3.1 Aerodynamic Development	7
	3.2 Compressor Mechanical Design	7
IV	Gasifier Turbine Development	9
	4.3 Ceramic Turbine Design and Development	9
	Gasifier Turbine Inlet Scroll	9
	Inner Backplates	9
	Gasifier Turbine Rotor	10
	Vanes	11
V	Power Turbine Development (no effort this period)	
VI	Combustor Development	17
	Test Facility	17
	Test Results	17
	Pilot	17
	Start Nozzle	18
	Main Nozzle	18
	Ceramic Components	19
VII	Regenerator Development	21
	Regenerator Cover	21
	Ceramic Exhaust Duct/Regenerator Seal Platform	22
	Regenerator Disk/Seal Performance	23
	First Engine Build	29
VIII	Secondary Systems	31
	8.1 Structures	31
	Combustion Case Assembly	31
	8.2 Gearbox and Power Transfer	33
IX	Materials Development	37
	9.1 Thermal Barrier Development	37
	Carborundum Effort	37
	Detroit Diesel Allison Effort	37
	9.2 Ceramic Component Development Characterization and Qualification	40
	Silicon Carbide Component Development	40
	Combustor Assembly	42

PAGE IV INTENTIONALLY BLANK

Section	Title	Page
	Gasifier Scroll Assembly	43
	Scroll Backplates	44
	Power Turbine Vanes	44
	Zirconia Component Development	44
X	Controls Development	47
XI	Transmission Development (transmission effort deleted)	
XII	Supportive Manufacturing, Cost, and Marketability	49
	12.1 Manufacturing Feasibility – Pontiac Motor Division	49
	12.2 Cost Analysis – Pontiac Motor Division	51
	Appendix A. Terms and Definitions	53

LIST OF ILLUSTRATIONS

Figure	Title	Page
1	1984 Pontiac Phoenix with gas turbine power train	3
2	AGT 100 engine cross section	3
3	Project schedule	4
4	Engine buildup sequence: hot section, showing combustor, scrolls, power turbine, and insulation	5
5	Engine buildup sequence: hot section, showing turbine exhaust duct/regenerator seal platform with combustor and scroll below	5
6	Estimated performance of BU1 and BU2 at 152 m (500 ft), 29.4°C (85°F)	6
7	Compressor impeller during inspection	7
8	Mock-up of revised gasifier scroll	9
9	Gasifier inner backplate analysis with worst-case bore cooling for one-piece design	9
10	Inner backplate modification to reduce thermal stress	10
11	Burst speed distribution characteristic for prototype gasifier turbine rotors	10
12	Three-dimensional finite element vane models	12
13	Gasifier vane temperature distribution at maximum power and steady-state conditions	12
14	Transient conditions used in analysis	12
15	Vane thermal response during transient condition	13
16	Gasifier vane contour plot of calculated transient temperatures	13
17	Gasifier vane contour plot of transient maximum principal stresses	13
18	Ceramic vane proof test rig	14
19	Vane thermal shock rig schedule for gasifier and power turbine	14
20	Comparison of gas inlet temperatures and wall temperatures during cyclic operation	15
21	Combustor assembly for first Mod I engine	17
22	Pilot test fixture	18
23	Combustor data for cycle point 8 at 65% speed	18
24	Failed ceramic dome	19
25	Regenerator cover	21
26	Load/deflection test setup for regenerator cover	21
27	Regenerator measured gas-side cold flow distributions at maximum power condition	23
28	Regenerator measured air-side cold flow distribution at maximum power condition	24
29	Regenerator air-side flow distribution testing	25
30	Ceramic exhaust duct/seal platform	26
31	Ceramic exhaust duct/seal platform pressure test rig	26
32	Exhaust duct/seal platform static stress test	27
33	Deflection test results of ceramic regenerator seal platform	27
34	Proof testing of ceramic exhaust duct/seal platform	28
35	Regenerator outboard seals with (a) nominal clamping force and (b) maximum clamping force	28
36	Development of alternate seals for BU1	28
37	Outboard seal leaf leakage for BU1	29
38	Comparative results of regenerator leakage testing	29
39	Regenerator drive torque and effectiveness for BU1 and alternate seal set	29
40	Regenerator system leakage for BU1	30
41	Regenerator effectiveness for BU1	30
42	Combustor case/inner gear case pressure test	31
43	Combustor case strain gage location	31
44	Inner gear case strain gage location	32
45	Stress at maximum stress locations for combustor case and inner gear case	32
46	Combustor housing stress summary	32
47	Deflection measurements of inner gear case	33
48	Failed harmonic drive unit	33
49	Regenerator drive gearbox – input side	34
50	Regenerator drive gearbox – output side	35
51	Microstructure of CBO mullite/cordierite	37
52	Microstructure of DDA zircon	38

Figure	Title	Page
53	Thermal expansion behavior of DDA zircon	38
54	Fracture origins in DDA zircon	39
55	Weibull plot for burst testing of gasifier rotors	40
56	Rotor shaft modifications	41
57	CBO gasifier rotors	41
58	Machined CBO combustor body	42
59	CBO combustor flame tube holders	42
60	CBO swirl plate after burner rig testing	43
61	CBO dilution bands	43
62	New gasifier scroll slip casting mold	44
63	Close tolerance gasifier rotor shrouds	44
64	Gasifier scroll assembly	45
65	Power turbine vanes	45
66	Zirconia components received from Kyocera	46
67	Output gear assembly	49
68	Present configuration of combustor case assembly	49
69	Proposed configuration of combustor case assembly	50
70	Inlet guide vane lever	50

LIST OF TABLES

Table	Title	Page
I	Thickness measurements	7
II	Prototype sintered alpha silicon carbide gasifier turbine rotors	11
III	Deflections of regenerator cover due to pressure loading	22
IV	Physical properties of CBO mullite	37
V	Phase character and properties for DDA zircon	38
VI	Processing yields of A and B quality prototype rotors	40
VII	Burst speeds for prototype rotors	40
VIII	MOR bar strength of prototype rotors	41
IX	Densities for gasifier rotors	41
X	Combustor bodies received January through July 1982	42
XI	NDE and quality assessment for CBO flame holders	42
XII	NDE status for CBO dilution bands	43
XIII	Dimensional measurements for two sintered outer backplates	44
XIV	Properties for AC Spark Plug zirconia	46

Summary

Engine/Power-Train Development

Fabrication of all parts was completed, and the first engine build was started. Only routine problems were encountered and the engine is scheduled to go to the test stand early in July.

Compressor Development

An inspection technique was employed on the Build No. 5 (BU5) impeller that uses a tracer and a comparator with master charts. Good correlation was achieved with micrometer measurements of the part. Compressor hardware was assembled for BU1 of the engine.

Gasifier Turbine Development

Activity has continued on ceramic hardware development. A revised scroll was designed, and eleven pieces were successfully slip cast. A revised inner backplate is indicated based on stress calculations that show high stresses at maximum-flow steady-state conditions. One hundred silicon carbide gasifier rotors have been made by the supplier and are in various stages of processing. Burst test results are encouraging and indicate that rotor quality is approaching that achieved in test bars. Finite element analyses of vanes indicate that an increase in strength of 54% is required to meet the design goal reliability without proof testing. Proof tests that result in a 2% rejection rate have been devised, however, and this approach appears acceptable.

Combustor Development

The combustor rig accumulated 26.5 hr of burning time during this reporting period. Testing included pilot-only, start-nozzle-only, and main-nozzle operation. During a bench test of the pilot nozzle assembly, satisfactory ignition was achieved for a wide range of starting speeds, and the lean blowout limit was as low as 0.06 kg/h (0.14 lb/hr) fuel flow. The centerbody start nozzle was tested to determine ignition characteristics and operation during the warm-up period at a range of burner inlet temperatures. It was determined that lean blowout was more closely related to nozzle atomization than to fuel/air ratio since the lean blowout limit was approximately 2.3 kg/h (5 lb/hr) regardless of airflow rate. For the main nozzle, five different cycle points were tested under steady-state conditions, three snap fuel transients were performed, and the transition from start nozzle fuel flow to main nozzle flow was investigated. This transition was accomplished manually without difficulty at burner inlet temperatures from 427°C (800°F) to 593°C (1100°F).

Regenerator Development

Regenerator parts were fabricated and qualification tested in preparation for the first engine build. Included were the regenerator cover, ceramic exhaust duct/seal platform, and regenerator disk/seal system. The regenerator system for the engine was assembled on schedule. Rig-based performance characteristics matched the first build requirements.

Secondary Systems

Harmonic drive gearbox rig testing resulted in three failures. No-load testing of the flex gear showed adequate life (6.6×10^6 cycles), but under load conditions failures were experienced. Analyses were inconclusive so an alternate design using a planocentric design scheme is being pursued.

Materials Development Summary

Mullite/cordierite thermal barrier materials being isopressed and sintered by Carborundum Co. (CBO) are showing reduced porosity, increased strength, and uniform composition. Zircon-based materials being developed by DDA show good coefficient thermal expansion (CTE) compatibility with silicon carbide and the highest strengths of all materials tested to date.

Component development work considered both silicon carbide and zirconia parts. A large effort went into characterizing the silicon carbide rotors. One hundred rotors have been received and inspected. Equivalent modulus of rupture (MOR) bar strengths were calculated from burst test results. These results agreed with laboratory results from radial-cut bars; values for axial-cut bars were lower.

Controls Development

The electronic control system has been checked out prior to engine test. All parts of the system have been fabricated new or modified from existing hardware, and special check-out equipment has been built as necessary. Control software has been programmed into the electronic control unit and was checked out using a test simulator.

Supportive Manufacturing, Cost, and Marketability

Manufacturing feasibility and cost analysis studies continue at Pontiac Motor Division (PMD) based on detailed engine component drawings received from DDA. PMD has now received 269 drawings defining the engine parts and assemblies. Many cost-saving design proposals have evolved from the manufacturing analysis studies conducted by PMD Manufacturing with input from DDA Engineering.

Introduction

This is one of a series of semiannual reports documenting work performed on an Advanced Gas Turbine (AGT) power-train system development project for automotive applications. The work is performed under NASA/DOE contract DEN3-168. The objective of the project is to develop an experimental power-train system that demonstrates (1) a combined cycle fuel economy of 17.9 km/L (42.5 mpg) using diesel fuel No. 2 in a 1984 Pontiac Phoenix of 1364 kg (3000 lbm) weight on a 15°C (59°F) day; (2) emission levels less than federal standards; and (3) the ability to use a variety of fuels. It is intended that the technology demonstrated through this project would assist the automotive industry in making a go/no-go decision regarding the production engineering development of gas turbine power trains. Figure 1 shows the Phoenix power train and objectives.

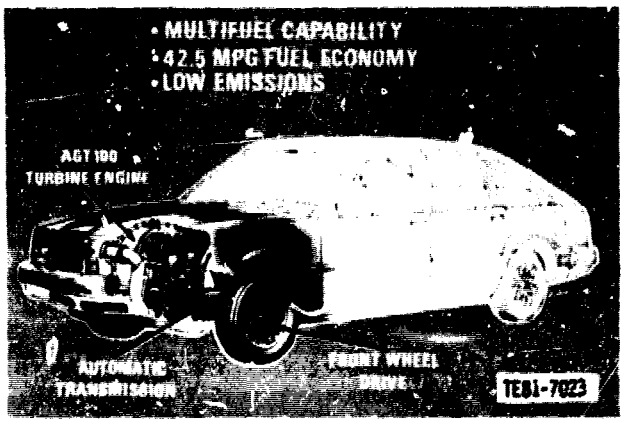

Figure 1. 1984 Pontiac Phoenix with gas turbine power train.

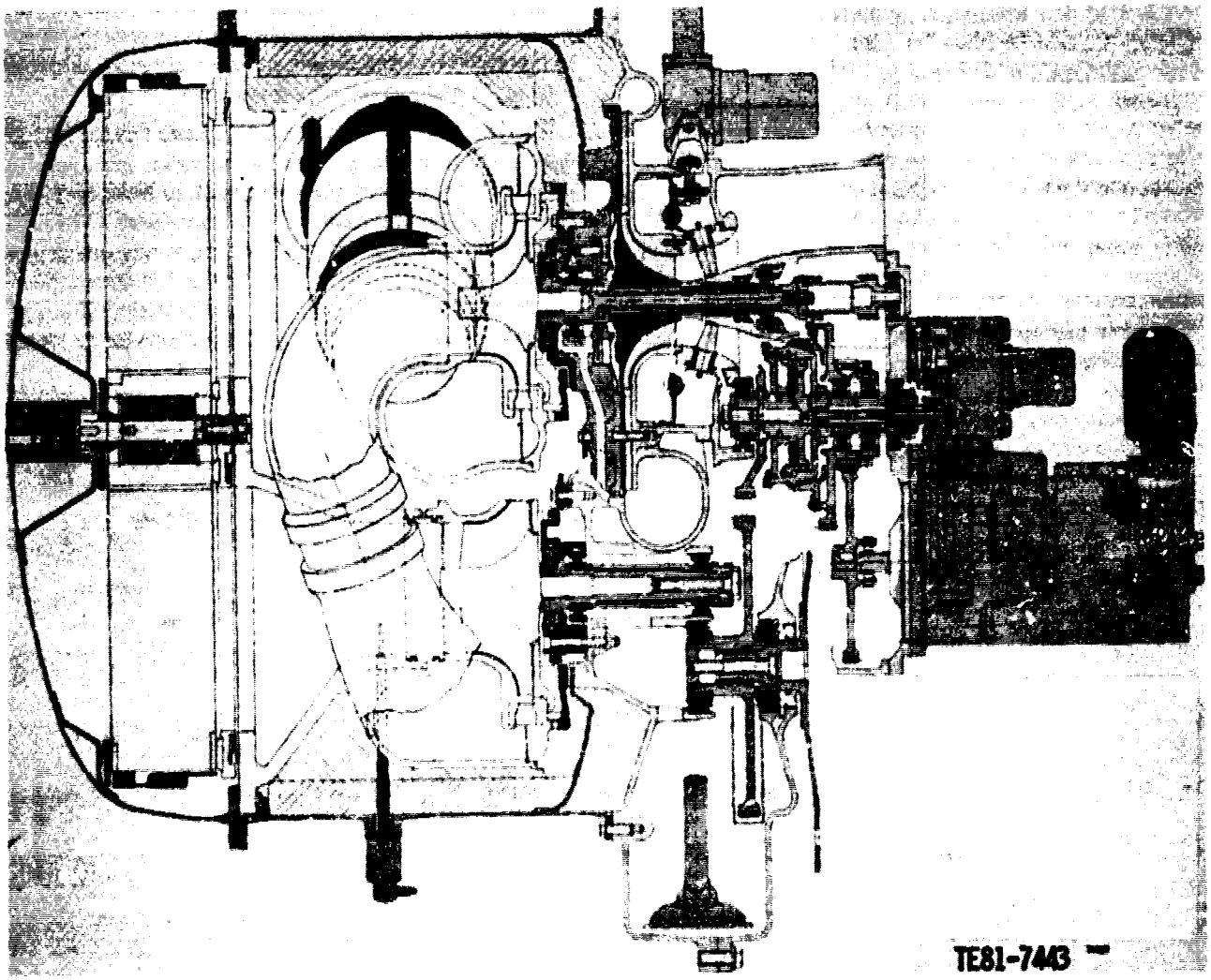

Figure 2. AGT 100 engine cross section.

PRECEDING PAGE BLANK NOT FILMED

In meeting the project objective, the design is constrained to (1) achieve reliability and life comparable to conventional 1985 vehicles; (2) achieve initial and life-cycle power-train costs competitive with 1985 power trains; (3) demonstrate vehicle acceleration suitable for safety and maneuverability; and (4) meet 1985 federal vehicle noise and safety standards. Figure 2 shows the engine cross section evolved to meet project objectives.

A team concept is used in this project, with many of the team members being General Motors Divisions. DDA is the prime contractor and team leader with responsibility for the overall power train and controls. Pontiac Motor Division (PMD) has vehicle responsibility. Delco Remy will develop the starter/boost system for the engine and Harrison Radiator Division is involved in the regenerator design and fabrication. The primary non-GM groups on the team are Carborundum Co. (CBO), Corning Glass Works (CGW), and GTE Laboratories Inc., who are involved in the ceramic effort.

The current project began in October 1979. Establishing and maintaining a reference power-train design (RPD) is a continuing activity as is component development.

The RPD is a preliminary engineering design of the power-train system that has the best potential for meeting the goals and objectives of the project. It can incorporate timely emerging technologies and will be updated as project activity progresses.

In this current program the RPD evolved from earlier studies and is presented as a concept of a fully developed production power train. The overall program plan is currently being reviewed and replanned to accommodate changes at DOE resulting from new direction by the Administration.

The main technology challenges in the program are in building small, high-performance gas turbine components and developing ceramic components for the required high engine cycle temperatures that are price competitive and can be produced in an automotive production environment. Because of the small-size engine (0.35 kg/s [0.76 lbm/sec] airflow), extensive rig testing is

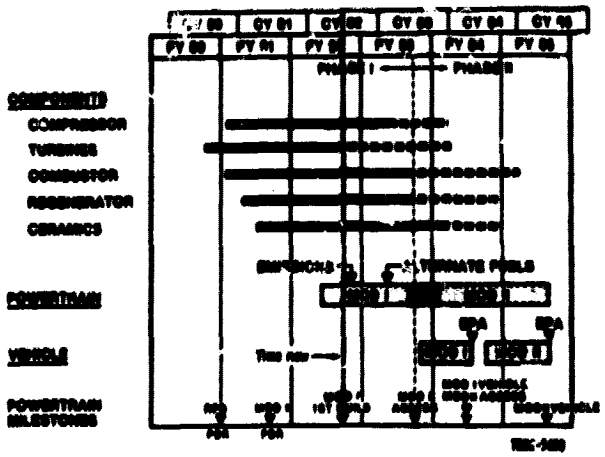

Figure 2. Project schedule.

being performed in component development. A major ceramic component development program is being pursued, and the ultimate success of the engine depends on the success of this activity. Figure 3 shows emphasis first on component development and then on proof of components in the engine and vehicle.

This report is structured on a component basis (e.g., all work relating to the gasifier turbine rotor, including rig work and ceramic rotor development, is discussed as a part of the gasifier turbine section). Exceptions to this are functional areas that are not peculiar to any one major component: engine subsystems, cover structures, gearbox and power transfer, rotor bearings, shafts/seals, and secondary flow. There are separate sections for materials development and controls development.

Certain sections are omitted in this report because no effort was expended in those areas. These sections—Vehicle System Development, Power Turbine Development, and Transmission Development—are identified in the Table of Contents to preserve continuity.

2.2 Mod I

Engine Build

Beginning in April the gas generator rotor and the power transfer clutch were assembled in accordance with a published engine assembly procedure. This specification provided engineering department instructions to supplement assembly drawings. It covered such items as assembly sequence, special measurements to determine shim selection, desired rotor build clearances, and procedures for measuring and obtaining the desired clearance.

In general, the build progressed at a rate normal for a first engine. The problems that were encountered along the way in most cases were typical of a first engine build and the result of one or more of the following causes: drawing interpretation; excessive manufacturing tolerance; interference due to tolerance stack; availability of parts; and deviation from normal assembly procedure because of special instrumentation.

The assembly problems normally were resolved by reworking the parts. This was accomplished via an Engineering Memorandum (EM) that instructed the shop to machine to a new set of dimensions and also instructed drafting to bring the drawing up to date with the rework. To ensure that all problems were documented and corrected, the inspection department filled out a Build Up Trouble Sheet form. This form has three headings: (1) problem description, (2) effect, and (3) corrective action. The first two items were filled in by the inspector, and a copy was sent to engineering. Engineering wrote the corrective action taken and returned the form to the inspection department. These detailed steps ensured that the problems were corrected and that changes were documented to prevent the same problem from arising again.

In addition to special instrumentation referred to above, the engine was built with greater than normal clearance and had rub pins installed on both turbine and compressor shrouds for the purpose of measuring the hot running clearance. This will establish the minimum clearances for future builds.

Figure 4 is a view of the engine looking from the regenerator and showing the assembly of the combustor, scrolls, and insulation. Figure 5 is the next step in the build sequence after Figure 4 and shows the regenerator seal platform/turbine exhaust duct installed. A photograph of the assembled engine is used as the frontispiece of this report.

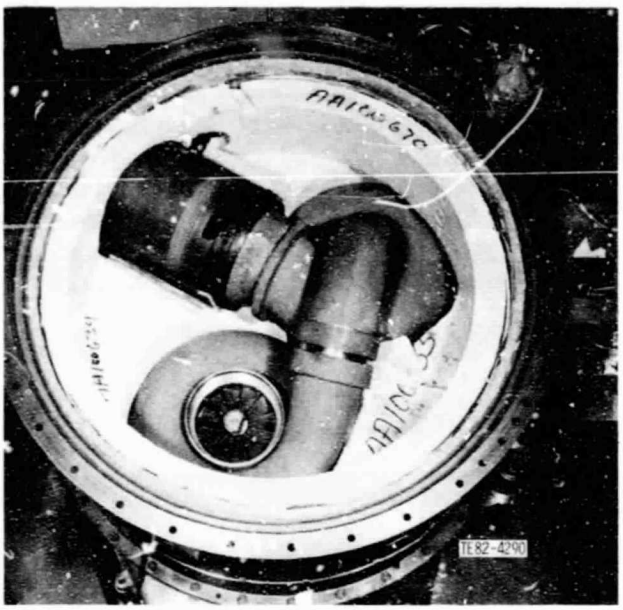

Figure 4. Engine buildup sequence: hot section, showing combustor, scrolls, power turbine, and insulation.

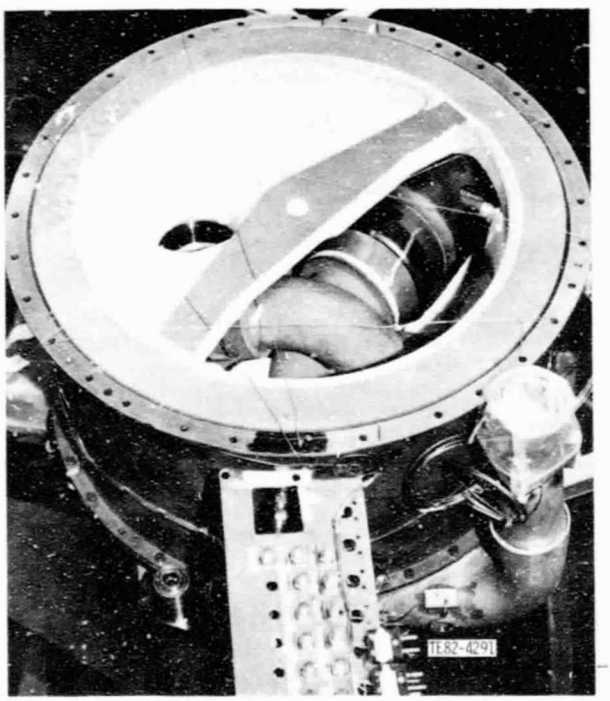

Figure 5. Engine buildup sequence: hot section, showing turbine exhaust duct/regenerator seal platform with combustor and scroll below.

In summary, all of the assembly problems to date have been resolved, the desired rotor clearances have been obtained, the engine build is completed, and the engine will be sent to the test stand early in July.

Performance

AGT 100 estimated performance is shown in Figure 6. These performance estimates are based on component rig test performance adjusted to the engine configuration. The engine development planned will improve the specific fuel consumption from the BU1 line shown to the Mod II specific fuel consumption shown over a three year period of time.

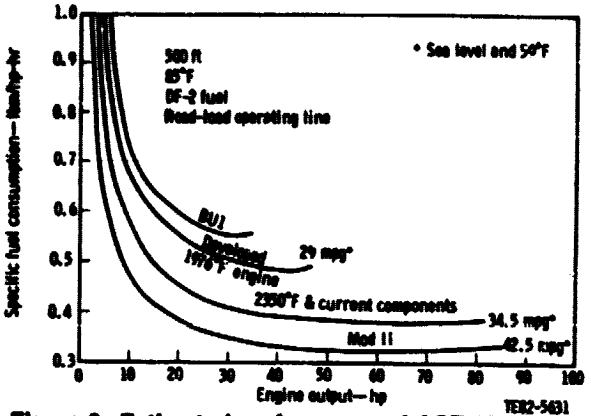

Figure 6. Estimated performance of AGT 100 engine.

III. Compressor Development

3.1 Aerodynamic Development

Compressor activities were limited to detail thickness measurement on the CX40 BU5 impeller. Measurements included both normal comparator chart and detail micrometer data. The CX40 BU5 impeller was inspected in the same manner as any new incoming impeller. This technique employs a tracer arrangement in which a small disk contacts the impeller along a predescribed plane in space. The shadow of the disk is projected onto a flat screen that holds the "master chart" (computer drawing) of the desired section plane. Direct contour and thickness measurements are made from these projections. Next, the blade, for which comparator chart data were available, was physically removed from the wheel. The individual blade, showing the measurement grid, is shown in Figure 7. Micrometer measurements were made at specified grid points in the master chart sections. These micrometer measurements were then compared with thickness measurements from the comparator chart. An extremely good correlation was seen to exist with the difference between the two forms of measurement being 0.025 to 0.064 mm (0.001 to 0.0025 in.). This comparison was needed to develop confidence for comparator chart measurements on small compressors.

The BU5 (thinned impeller) comparator chart was compared with the BU3 (original impeller) chart, and the results are shown in Table I.

The intent of the BU5 rework was to reduce the blade thickness by a uniform 0.254 mm (0.010 in.). The data shown in Table I indicate a much greater stock removal than desired.

3.2 Compressor Mechanical Design

Component testing of the hex-type mass isolator springs revealed that the spring rate was lower than calculated for all three positions. New isolator springs of the segmented type were made but they too were low in spring rate. It was decided to run the initial build of the engine with the segmented type springs and to investigate the analytical model for calculating the spring rates. When the problem with the program has been resolved, new mass insolator springs will be procured.

The compressor shroud was recontoured in the knee area so that acceptable tip running clearance could be obtained. Engine hardware was also reworked to provide instrumentation for performance evaluation.

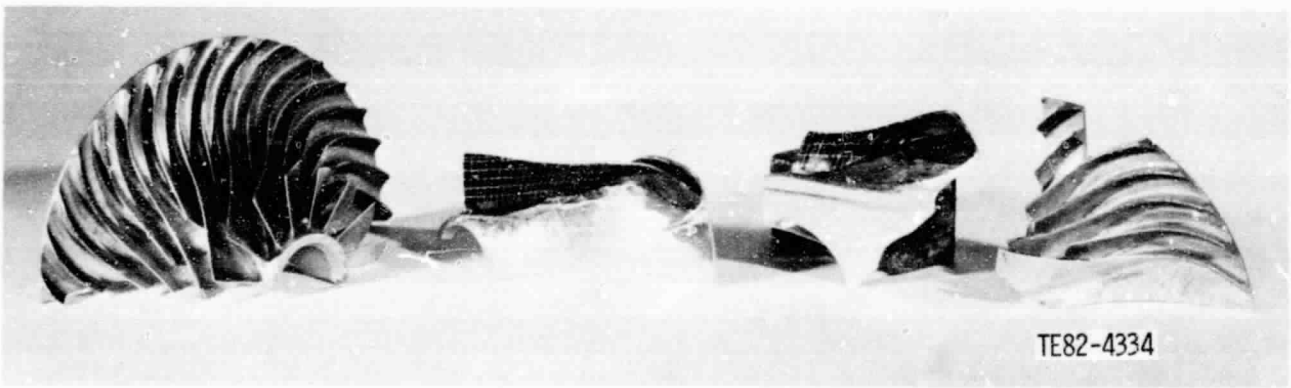

Figure 7. Compressor impeller during inspection.

Table I. Thickness measurements.

	Hub		Shroud	
	mm	in.	mm	in.
BU3	+ (0.076-0.102)	+ (0.003-0.004)	+ (0.102-0.127)	+ (0.004-0.005)
BU5	– (0.356-0.406)	– (0.014-0.016)	– (0.203-0.229)	– (0.008-0.009)
BU3-BU5	(0.431-0.508)	(0.017-0.020)	(0.305-0.356)	(0.012-0.014)

*Relative to the "as designed" Master Charts.

4.3 Ceramic Turbine Design and Development

Gasifier Turbine Inlet Scroll

A design of a slip cast sintered alpha silicon carbide gasifier turbine scroll has been released for fabrication. An epoxy mold and pattern were produced, and examination indicated that a number of thin plaster inserts would be needed to generate the inlet transition of the scroll. To improve potential yield, a redesign of this area was undertaken with the objective of reducing the number and increasing the size of the inserts.

The redesign has been accomplished without significant modification of the aerodynamically desired flow area progression. A mock-up of the revised shape is shown in Figure 8. The epoxy pattern has been modified, and plaster molds have been formed from it. To date 22 scrolls have been slip cast, and 11 have minor or no cracks. Two scrolls with minor flaws are currently being baked and sintered.

Inner Backplates

The inner backplate forms the flow-path boundary at the back side of each turbine rotor in the AGT 100 engine and, because of high temperatures in the RPD version, will be made of ceramic material. Several sample pieces have been isopressed and machined out of sintered alpha silicon carbide. Detailed finite element analyses have been undertaken to determine suitability for incorporation in the initial engine build. The results indicate that with worst case assumptions relative to coolant mixing at the bore, a large radial temperature gradient and high stress levels occur at maximum-flow steady-state conditions. With the current material strength properties of modulus of rupture (MOR) = 344.7 MPa (50 ksi) and Weibull modulus (m) = 8, a low probability of survival is predicted. Probability of survival is 0.003 for the gasifier turbine and 0.532 for the power turbine.

Stress and temperature distribution are shown in Figure 9 for the gasifier turbine inner backplate. A decision has been made to machine metal versions of the inner backplates for use in Mod I testing while potential solutions are explored analytically. One promising approach is to separate the central portion of the backplate to reduce the radial stiffness. Figure 10 shows this approach. Using the same material strength level, the computed probability of survival is significantly improved.

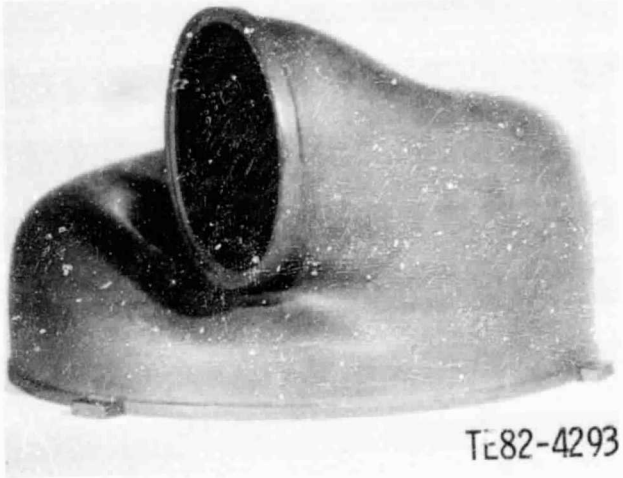

Figure 8. Mock-up of revised gasifier scroll.

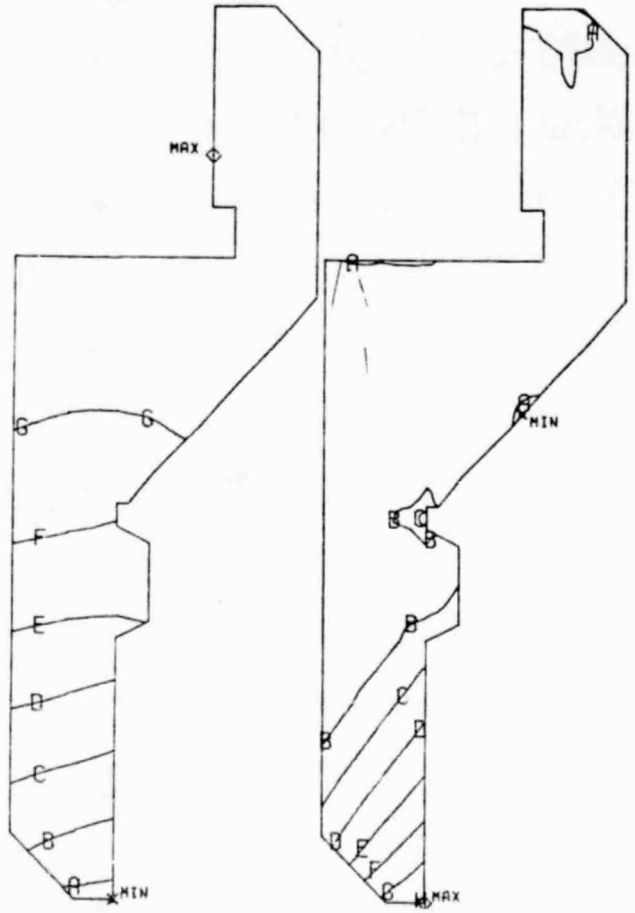

TEMPERATURE

	F	C
A	2000.0	1093.33
B	2040.0	1115.56
C	2080.0	1137.78
D	2120.0	1160.00
E	2160.0	1182.22
F	2200.0	1204.44
G	2240.0	1226.67
MAX	2267.7	1242.04
MIN	1987.3	1086.30

MAX PRINCIPAL STRESS

	KSI	MPA
A	0	0
B	7.0	48.26
C	14.0	96.53
D	21.0	144.73
E	28.0	193.05
F	35.0	241.32
G	42.0	289.58
H	49.0	337.84
MAX	50.2	346.44
MIN	-.1	-.76

Figure 9. Gasifier inner backplate analysis with worst-case bore cooling for one-piece design.

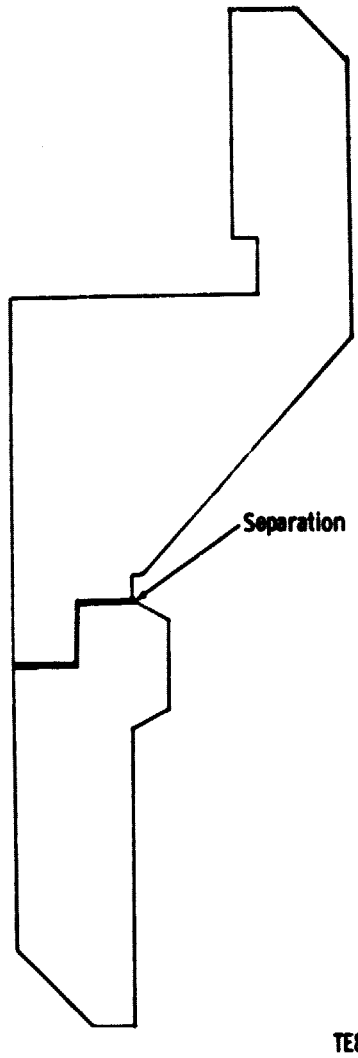

Figure 10. Inner backplate modification to reduce thermal stress.

Probability for survival becomes 0.97 for the gasifier turbine and 0.9996 for the power turbine. This modification can be accomplished using existing parts and may be incorporated in the engine after suitable proof testing.

Gasifier Turbine Rotor

Manufacture of prototype sintered alpha silicon carbide gasifier turbine rotors by Carborundum has been completed, and tooling for the engine part has been procured. One hundred engine rotors have been molded and are in various stages of processing.

Characterization of the prototype rotors has also been completed. The last 33 rotors received from Carborundum represent a matrix of minor process variations in an attempt to improve quality and yield. Table II shows rotor serial numbers and the coded process variables. All rotors received were inspected and graded for quality based on visual and fluorescent penetrant inspection (FPI) indications. Three broad categories for sorting were used as follows:

"A" meets drawing specifications and has no linear indications nor major porosity
"B" minor defects that can be removed by hand blending
"C" too numerous or severe nondestructive evaluation indications that cannot be satisfactorily removed by hand blending

"A" and "B" quality rotors were deemed acceptable for spin testing. "C" quality rotors were used for cut-up (materials evaluation) and display purposes.

The burst test results are also listed in Table II. It is interesting to note that the highest burst speeds corresponded to those variables with the highest quality yield. Composition No. 3, atmosphere No. 2, and sintering treatment No. 9 all had a higher percentage of "A" rotors than other variables. The two highest burst speeds came from rotors fabricated with these variables.

The distribution of burst speeds of the 15 rotors that were burst has been evaluated. The data were fitted to a two-parameter Weibull distribution using median ranking and least squares regression with reasonable success ($r = 0.97$) as shown in Figure 11.

Recognizing that, in the test, stress is proportional to the square of speed, a material strength Weibull modulus can be deduced as one-half the plot slope (see Figure 11). In this case the plot slope is 14.51 and the underlying strength Weibull modulus is approximately 7.25. Assuming this modulus and the median burst speed of 97,000 rpm, an equivalent MOR strength was computed in an iterative fashion using an available axisymmetric finite element model. The results show an approximate equivalent MOR bar strength of 340 MPa (49.3 ksi). This indicates that rotor strength is approaching that achieved in test bars.

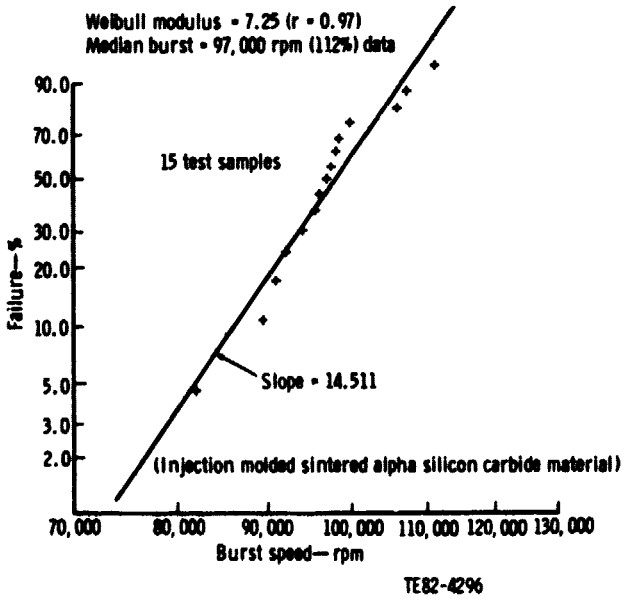

Figure 11. Burst speed distribution characteristic for prototype gasifier turbine rotors.

Table II. Prototype sintered alpha silicon carbide gasifier turbine rotors.

DDA S/N	CBO S/N	Qlty	Composition No.	Batch No.	Presinter No.	Atmosphere No.	Sinter No.	Density—g/cm³	Burst speed—rpm
FX24868	404		2	1	1	2	1	3.15	98,500
FX24869	405		2	1	1	2	1	3.14	
FX24870	407	C	2	1	1	2	1	3.14	
FX24871	408	C	2	1	1	2	1	3.14	
FX24872	410		2	2	2	2	2	3.13	95,000
FX24873	411		2	2	2	2	2	3.12	89,500
FX24874	412		2	2	2	2	1	3.12	91,000
FX24875	414		2	2	2	2	2	3.08	100,000
FX24876	415	C	2	2	2	2	2	3.09	
FX24877	420	C	2	2	2	2	3	3.13	
FX24878	424	B	2	2	2	2	3	3.14	94,000
FX24879	425	C	2	2	2	2	3	3.13	
FX24880	465	A	2	3	1	2	7	3.07	97,000
FX24881	466	C	2	3	1	1	7	3.08	
FX24883	468	C	2	3	1	1	7	3.08	
FX24884	470	C	2	3	1	1	7	3.09	
FX24885	488	C	1	5	1	1	7	2.97	
FX24886	459		2	3	1	1	5	3.09	
FX24887	453	C	2	3	1	1	5	3.10	
FX24888	437	B	2	1	1	2	8	3.13	96,000
FX24889	438	A	2	1	1	2	8	3.12	106,000
FX24890	439	A	2	1	1	2	8	3.13	97,600
FX24891	419	C	2	1	1	2	4	3.13	
FX24892	442	C	2	1	1	2	8	3.12	
FX24893	445	A	2	1	1	2	8	3.13	82,000
FX24894	472	B	3	6	1	2	8	3.11	98,000
FX24895	475	A	3	6	1	2	9	3.07	92,000
FX24896	497	C	1	5	1	1	6	3.07	
FX24897	476	A	3	6	1	2	9	3.12	107,700
FX24898	477	A	3	6	1	2	9	3.08	111,500
FX24899	483	B	3	6	1	2	10	3.13	
FX24900	487	C	3	6	1	2	10	3.14	
FX24901	500	C	1	4	1	2	10	3.09	

Vanes

Detailed three-dimensional finite element analyses of the gasifier and power turbine vanes have been initiated. Figure 12 depicts both finite element models. The gasifier vane has been analyzed at both steady-state and transient conditions. Steady-state analysis at maximum power shows minimal thermal gradients (see Figure 13) and negligible stress levels. Transient analysis was performed using the temperature and flow schedules in Figure 14.

The transient analysis did detect considerable thermal gradients. The most severe condition occurs approximately 16 sec (see Figure 15) after the onset of the transient. Temperature and stress distributions at this point are shown in Figures 16 and 17. The gradient noted is due primarily to endwall effects since the vane is situated in pockets at both ends. A two-dimensional finite element model of the turbine scroll and backplate was used to establish the thermal boundary conditions in these pockets during the transient and is felt to be fairly accurate. In addition, the results are quite similar to analysis of the CATE gasifier vane.

Weibull material parameters were used to evaluate vane reliability. The parameters used are shown here and are representative of early sintered alpha silicon carbide MOR bars tested at DDA.

Characteristic strength— MOR = 343 MPa (49.7 ksi) (4-pt bend)		Weibull modulus, m
Unit volume	176 MPa (25.58 ksi)	8.43
Unit surface area	335 MPa (48.60 ksi)	8.71

The computed reliability is shown below:

Volume	0.9891
Surface	0.9908
Total	0.9800

A design goal of 0.9994 probability of survival has been established for the vane based on reliability allocation. To meet this requirement without a proof test, the

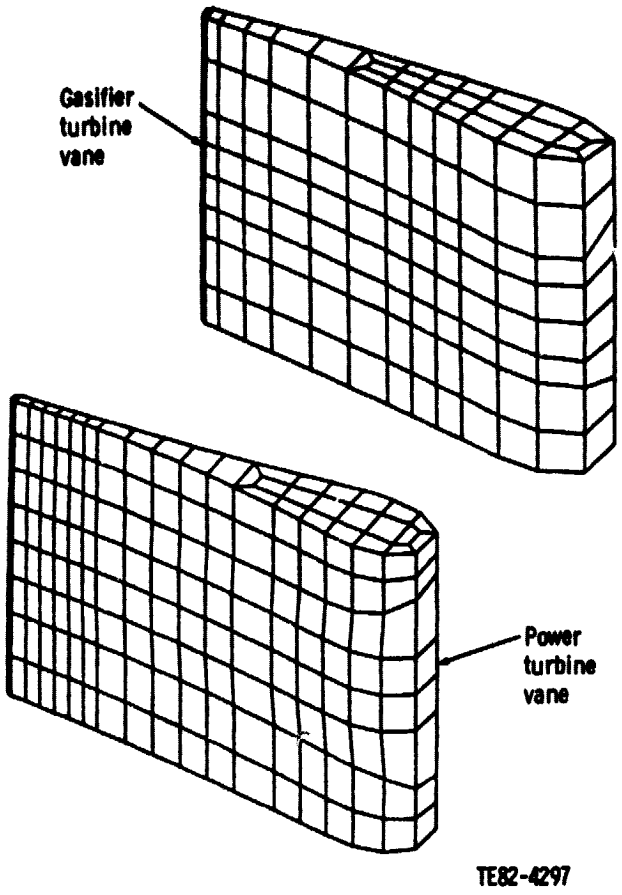

Figure 12. Three-dimensional finite element vane models.

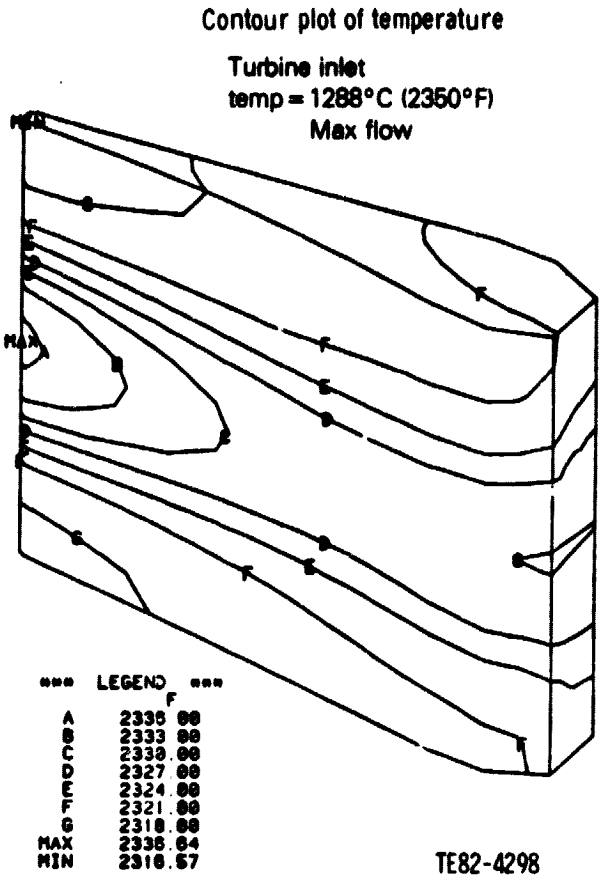

Figure 13. Gasifier vane temperature distribution at maximum power and steady-state condition.

strength would have to improve 54% at a Weibull modulus of 8. An alternate means of achieving satisfactory reliability would be to use a proof test simulating transient conditions. Such a test should result in a 2% rejection rate with the properties used in the analysis and would appear to be acceptable.

A proof test for the ceramic vanes has been devised in an attempt to screen vanes for engine tests. A simple test section for both the gasifier and power turbine vanes has been fabricated and adapted to an existing combustion rig previously used for regenerator core sample tests. The test section has a capacity for simultaneous evaluation of three vanes. The vanes are placed in a linear stagger as shown schematically in Figure 18. The spacing simulates the aerodynamic "throat" or flow capacity of the engine. The linear stagger was selected to maintain proper flow incidence and to simplify the test section.

A transient schedule for both vanes has also been devised and is shown in Figure 19. Eighteen ceramic (sintered alpha silicon carbide) gasifier vanes and 21 power turbine vanes have been qualified in the rig using the Mod I temperature schedule, and no failures have occurred.

The test is thought to be more severe than the engine because the vanes are tested with the ends unmachined,

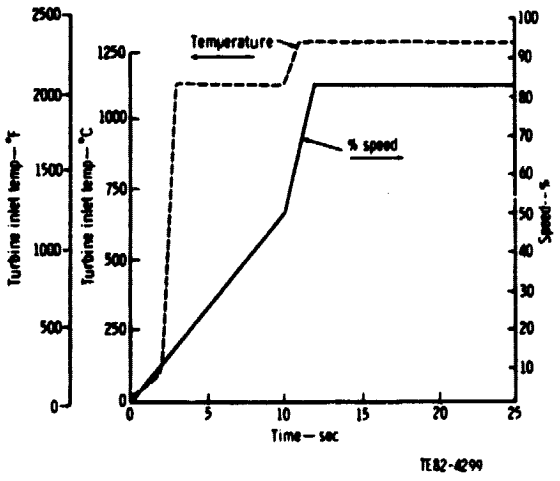

Figure 14. Transient conditions used in analysis.

and more than 5 mm of the vane ends are buried in cooled metal endwalls. Furthermore, the testing subjected the vanes to considerable burner noise. Figure 20 depicts a typical test thermal profile. In view of the results, future testing will be conducted at the 1288°C (2350°F) RPD level rather than the 1093°C (2000°F) Mod I level.

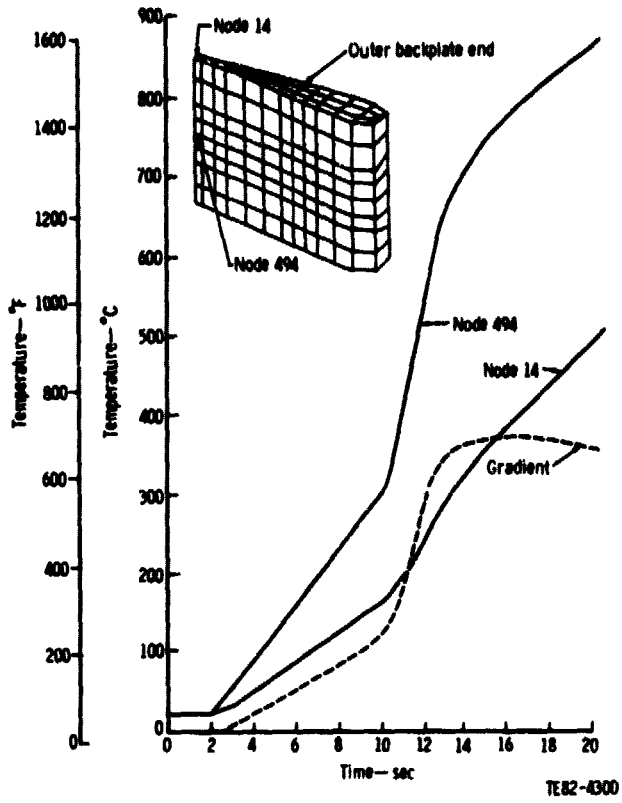

Figure 15. Vane thermal response during transient condition.

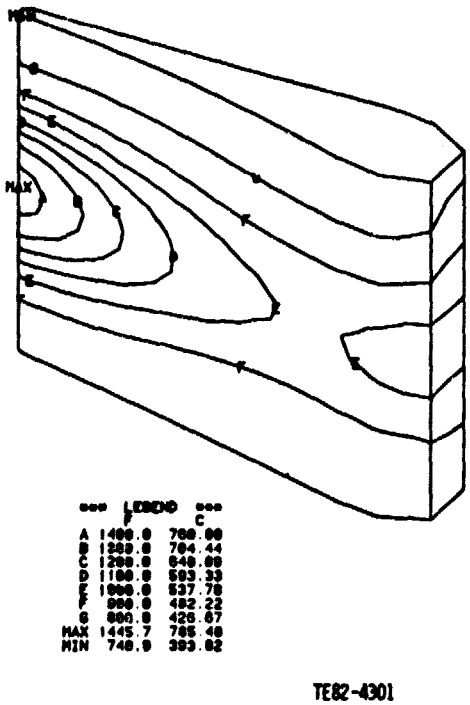

Figure 16. Gasifier vane contour plot of calculated transient temperatures.

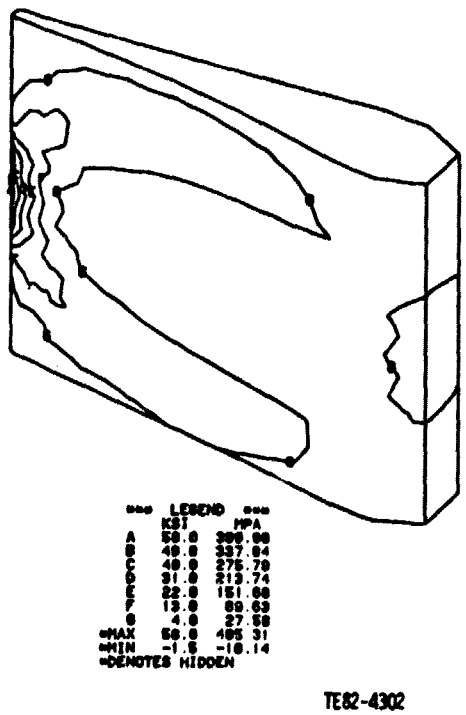

Figure 17. Gasifier vane contour plot of transient maximum principal stresses.

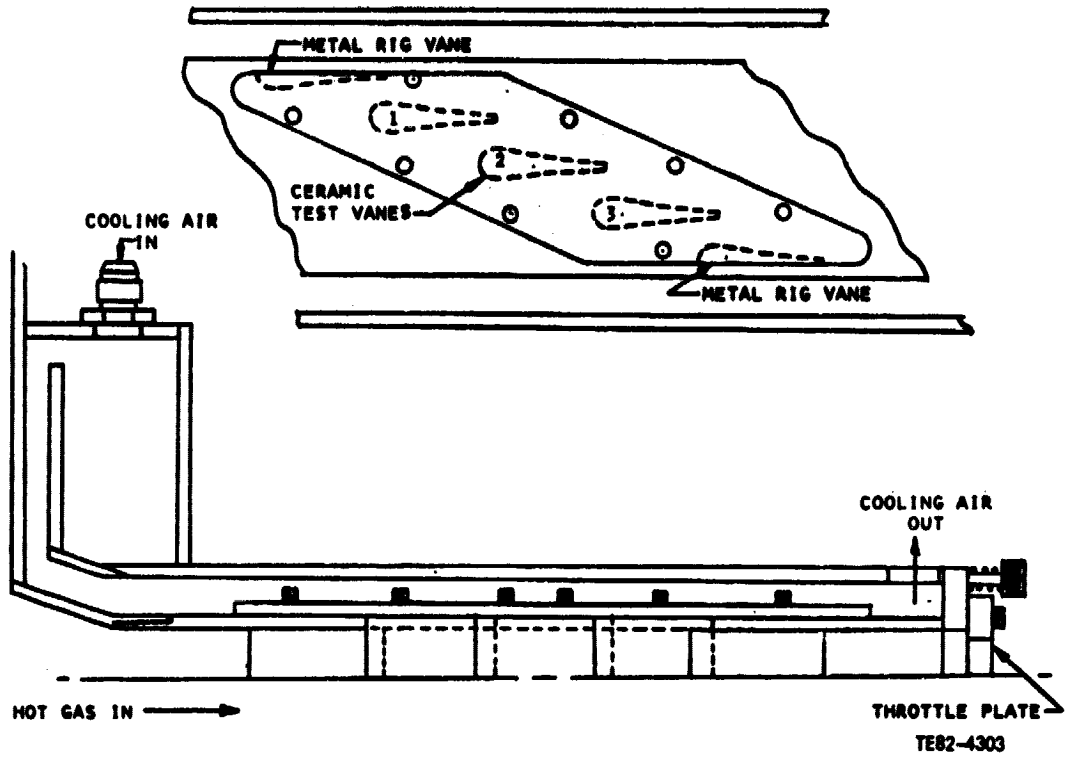

Figure 18. Ceramic vane proof test rig.

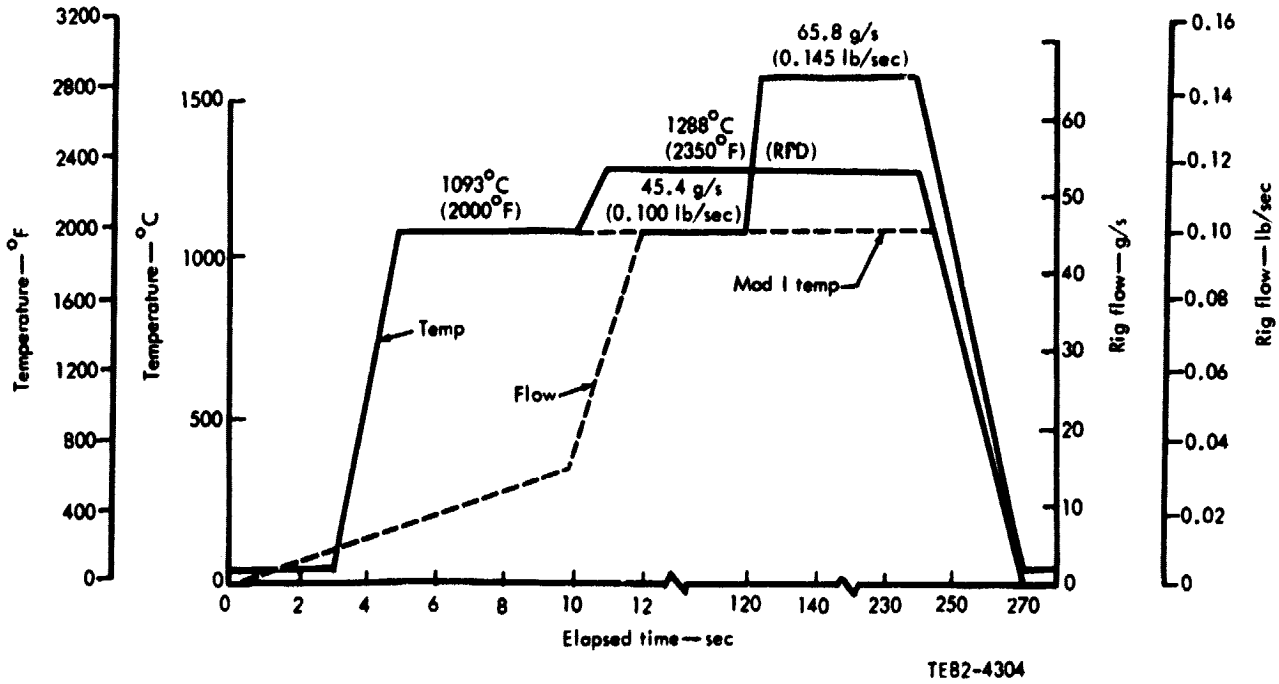

Figure 19. Vane thermal shock rig schedule for gasifier and power turbine.

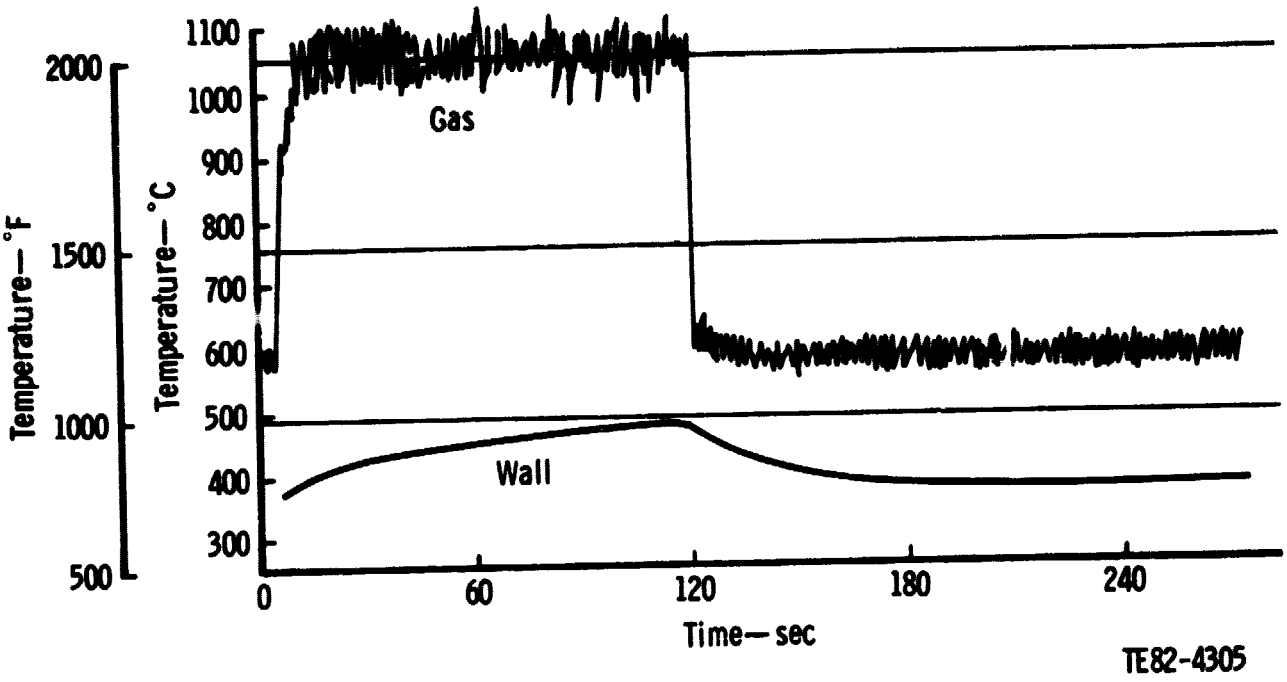

Figure 20. Comparison of gas inlet temperatures and wall temperatures during cyclic operation.

VI. Combustor Development

Test Facility

The combustor for the first Mod I engine differed slightly in design from the prototype model previously tested. Some rework of the combustor rig was necessary before the new design could be tested. The revision to the rig was limited to the hardware associated with the combustor inlet airflow path, the igniter location, the variable geometry linkage, and the combustor exit seal. Four new platinum/platinum-rhodium thermocouple rakes were installed in the exhaust instrumentation section, replacing the temporarily installed chromel/alumel thermocouples.

After the reworked rig and combustor were installed, minor problems were encountered with the variable geometry operation. These problems were corrected by increasing the clearance between the prechamber centerbody and the radial swirler. No other significant operational problems were encountered with the rig. There was a facilities problem, however; a leak developed within the high-temperature preheater, causing a significant reduction in the airflow reaching the combustor. After completing the testing required for the first engine build, the preheater core was removed and returned to the vendor for evaluation and repair.

Test Results

During this reporting period, 26.5 hr of burning time were accumulated on the combustion rig. That time was divided among pilot-only operation (5 hr), start-nozzle-only operation (8.5 hr), and main-nozzle operation (13 hr). A photograph of the combustor assembly, including the three fuel nozzles, is shown in Figure 21.

Pilot

An aluminum housing was fabricated for a bench test of the pilot nozzle assembly to investigate ignition and combustion characteristics. This fixture positioned the igniter, dome, fuel nozzle, and ceramic flame tube exactly as they would be in either the rig or in the engine. A photograph of this test fixture showing the pilot nozzle in operation at about 0.14 kg/h (0.3 lb/hr) fuel flow is shown in Figure 22.

The fixture was connected to an air supply that was adjusted to give a pressure drop across the pilot equal to the expected liner drop during engine starting. An orifice was sized to limit the air entering the pilot combustion chamber so that satisfactory ignition could be achieved over a wide range of starting speeds. The ignition limits

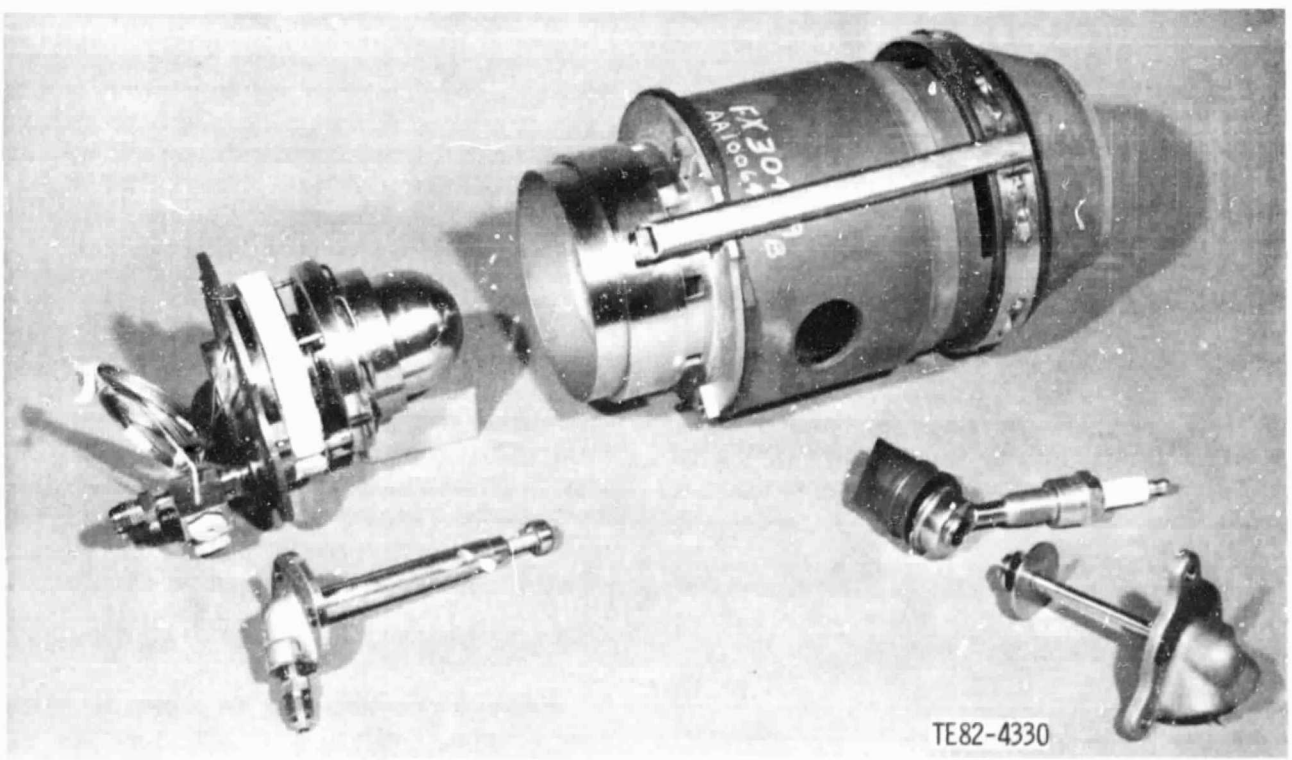

Figure 21. Combustor assembly for first Mod I engine.

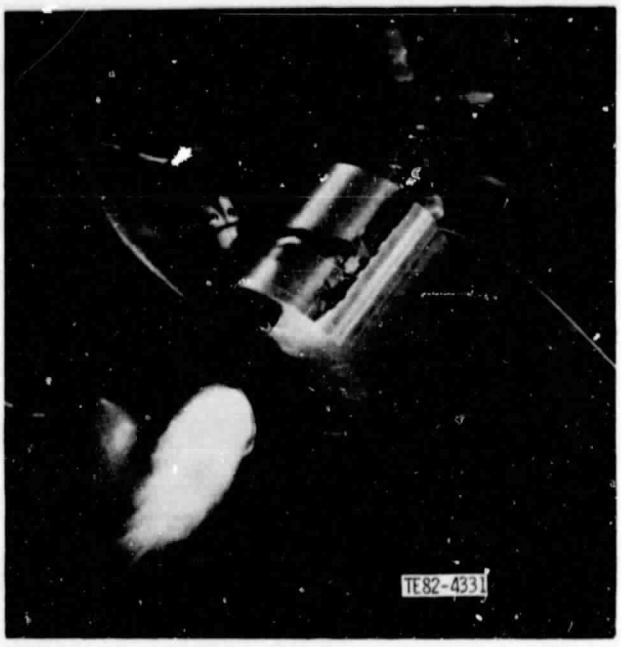

Figure 22. Pilot test fixture.

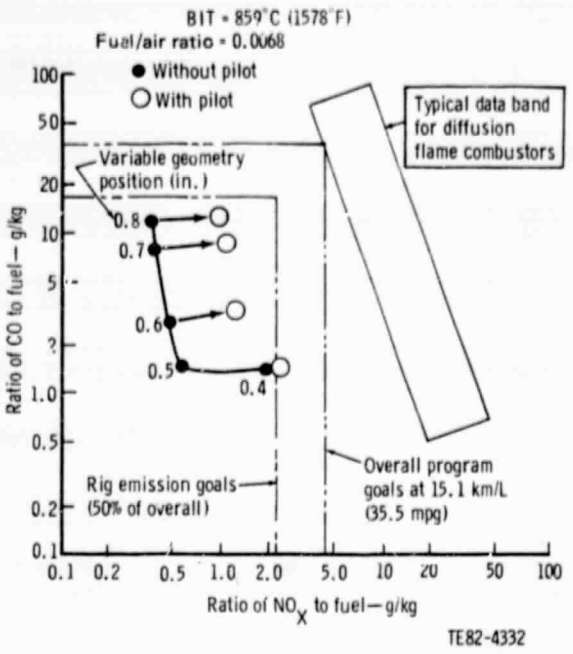

Figure 23. Combustion data for cycle point 8 at 65% speed.

were quite wide, and lean blowout was as low as 0.06 kg/h (0.14 lb/hr) fuel flow.

Start Nozzle

The centerbody start nozzle was tested to determine ignition characteristics and lean blowout limits at starting conditions. It was also tested over a range of inlet temperatures up to a burner inlet temperature (BIT) of 538°C (1000°F) to simulate operation during the warm-up period.

Fuel from the start nozzle was ignited quite reliably from an established pilot flame over a range of start nozzle fuel flows and simulated engine operating speeds. Airflows corresponding to engine speeds of 25% to 45% were tested, and fuel flow necessary for ignition ranged from 2.3 to 3.6 kg/h (5 to 8 lb/hr). Lean blowout was approximately 2.3 kg/h (5 lb/hr) regardless of airflow rate, indicating that lean blowout was more a function of nozzle atomization than fuel/air ratio (the nozzle ΔP was approximately 62 kPa at 2.3 kg/h (9 psi at 5 lb/hr).

Two improvements were made in the operation of the centerbody start nozzle. First, it was found that opening the variable geometry and allowing more air to enter the primary zone improved the burner outlet temperature (BOT) profile. In addition, the minimum fuel flow necessary to achieve reliable ignition decreased as the variable geometry was opened, up to an opening of 7.6 mm (0.3 in.). Starts were made successfully with the geometry as open as 17.8 mm (0.7 in.) although more fuel flow was required.

A second improvement was made to the starting characteristics by supplying additional air to the centerbody cavity. This air flowed from the cavity through the swirler surrounding the fuel nozzle tip and provided an air assist to the fuel atomization. A significant improvement was made at an air supply pressure differential of only 1.7 kPa (0.5 in. Hg), and slight additional improvement was noted as the pressure difference was increased to 1.7 kPa (1.5 in. Hg). The lean blowout limit for the start nozzle was reduced to about 1.4 kg/h (3 lb/hr) when 1.7 kPa (0.5 in. Hg) was supplied to the centerbody.

The start nozzle was evaluated during a simulated warm-up period. The airflow was kept constant at 0.08 kg/s (0.18 lb/sec), equivalent to idle speed, while the inlet temperature was allowed to increase from an initial level of 204°C (400°F) to a final level of 538°C (1000°F). During that time the start nozzle fuel flow was adjusted to maintain a BOT of approximately 982°C (1800°F).

Main Nozzle

Five different cycle points were tested under steady-state conditions, three snap fuel transients were performed, and the transition from start nozzle fuel flow to main nozzle flow was investigated. Emissions were measured for the steady-state conditions for multiple settings of the variable geometry and for operation both with and without the pilot flame. Figure 23 shows typical results for this combustor at 65% speed. At this operating condition, adjustment of the variable geometry from 10.2 mm (0.4 in.) to full open, 22.9 mm (0.9 in.), was possible without adversely affecting the combustor operation.

The measured emissions and the appearance of the flame were very similar to previous tests with the prototype combustor even though an appreciably different fuel injection design was used.

The total fuel flow for the operating condition shown in Figure 23 was approximately 3.1 kg/h (6.8 lb/hr). When 0.27 kg/h (0.6 lb/hr) of this total fuel flow was burned in the diffusion flame pilot nozzle, the NO_x emissions increased nearly 2.5 times over the level measured when all the fuel was burned in the premix/prevaporization mode.

The combustors tested during this period used the slotted dome design. These slots, which were added to relieve the thermally induced stresses, apparently caused no significant changes to the aerodynamic performance of the combustor. During some operation, however, diffusion flame combustion was observed in the vicinity of the slots, as unvaporized fuel was slung through the slots from the prechamber. This situation was most noticeable during operation with low inlet temperature or with high primary zone fuel/air ratio.

Transition from the start to the main nozzle was accomplished manually on the rig without difficulty at burner inlet temperatures from 427°C to 593°C (800°F to 1100°F). The only problem observed was that combustion occurred very near the dome slots for a short period of time when the inlet temperature was low. Operation at low inlet temperature was enhanced by decreasing the fuel manifold cooling rate and thereby increasing the fuel temperature at the nozzle.

Ceramic Components

The combustor shown in Figure 21 has four ceramic components: the dome, the main body, the dilution band, and the pilot flame tube. The design of the combustor body and the slotted dome described above constitute the major differences between the ceramic components of this combustor and the prototype combustor previously tested. The body in the current design consists of a single piece of ceramic, which replaces the two-piece body used in the prototype. The external shape of the body in the new design is approximately the same as the prototype, but it employs a different seal arrangement at the combustor exit.

After each day of testing, the combustor centerbody was removed and the interior surface of the ceramic was visually inspected. No damage was observed through the first six days of testing; however, after the seventh day, a crack was observed in the dome. During the seventh test day, two major failures in the test hardware occurred that could have led to the dome failure. First the air leak in the preheater became more obvious, especially at the low inlet temperature, and caused a considerable decrease in actual airflow through the combustor. As a result, excessively rich combustion occurred for some time in the burner, leaving a sizable deposit of carbon. At approximately the same time, a leak developed in the coolant flow path surrounding the main nozzle that permitted water to leak into the combustor rig. When the combustor was inspected the next day, the rig was almost completely filled with water. Whether either of these operational failures caused the crack in the dome is a matter of conjecture. It is certain, however, that the conditions of the test were unusual and undoubtedly more difficult than would be expected in actual engine operation. A photograph of the cracked dome is shown in Figure 24.

The combustor was tested one more day after the crack in the dome was discovered and before it was removed. Upon close inspection of the components after removal, a small crack (about 13 mm [0.5 in.] long) was also found on the outside of the combustor body.

Another assembly, consisting of a new dome, body, and dilution band, was installed in the rig for additional proof testing. Nearly 4 hr of burning time were accumulated on this assembly, including the snap fuel transient operation. No damage was observed in any of these ceramic components after the rig testing.

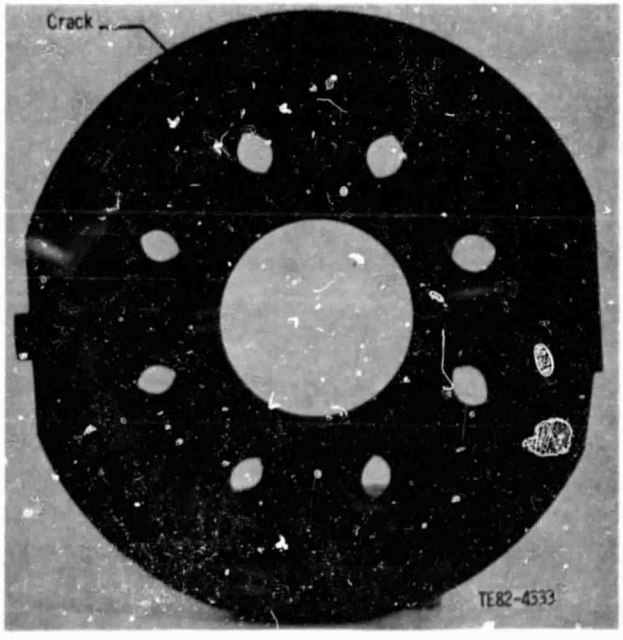

Figure 24. Failed ceramic dome.

"Page missing from available version"

"Page missing from available version"

Table III. Deflections of regenerator cover due to pressure loading.

Pressure— kPa	Position No. 1	2	3	4	5	6	7	8	9	10	11	12
						Deflections in mm						
0	0	0	0	0	0	0	0	0	0	0	0	0
68.9	0	0	0	0	0	0	0	0	0	0	0	0
137.9	0.0127	0	0	0	0	0	0	0	0	0	0	0
206.9	0.0051	0.0051	0	0.0254	−0.0127	0	0.0051	0.0330	−0.0051	0.0051	−0.0254	0
275.8	0.0762	0.0254	0	0.0381	−0.0254	0	0.0203	0.0762	−0.0178	0.0203	−0.0254	−0.0254
344.8	0.1041	0.0381	−0.0076	0.0635	−0.0330	0	0.0305	0.1016	−0.0254	0.0254	−0.0254	−0.0254
379.2	0.1219	0.0406	−0.0076	0.0762	−0.0381	0	0.0381	0.1143	−0.0279	0.0406	−0.0254	−0.0254
310.3	0.1016	0.0483	−0.0076	0.0610	−0.0381	0	0.0330	0.1016	−0.0254	0.0254	−0.0254	−0.0254
241.3	0.0762	0.0457	−0.0051	0.0457	−0.0254	0	0.0279	0.0762	−0.0178	0.0178	−0.0254	−0.0203
172.4	0.0508	0.0203	−0.0051	0.0203	−0.0178	0	0.0203	0.0508	−0.0127	0.0127	0.0127	0
103.4	0.0254	0.0051	0	0	0	0	0.0203	0	0	0	0.0051	0
0	0.0127	0	0	0	0	0	0	0	0	0	0	0

Pressure— psig	Position No. 1	2	3	4	5	6	7	8	9	10	11	12
						Deflections in thousandths of inches						
0	0	0	0	0	0	0	0	0	0	0	0	0
10	0	0	0	0	0	0	0	0	0	0	0	0
20	0.5	0	0	0	0	0	0	0	0	0	0	0
30	0.2	0.2	0	1.0	−0.5	0	0.2	1.3	−0.2	0.2	−1.0	0
40	3.0	1.0	0	1.5	−1.0	0	0.8	3.0	−0.7	0.8	−1.0	−1.0
50	4.1	1.5	−0.3	2.5	−1.3	0	1.2	4.0	−1.0	1.0	−1.0	−1.0
55	4.8	1.6	−0.3	3.0	−1.5	0	1.5	4.5	−1.1	1.6	−1.0	−1.0
45	4.0	1.9	−0.3	2.4	−1.3	0	1.3	4.0	−1.0	1.0	−1.0	−1.0
35	3.0	1.8	−0.2	1.8	−1.0	0	1.1	3.0	−0.7	0.7	−1.0	−0.8
25	2.0	0.8	−0.2	0.8	−0.7	0	0.8	2.0	−0.5	0.5	0.5	0
15	1.0	0.2	0	0	0	0	0.8	0	0	0	0.2	0
0	0.5	0	0	0	0	0	0	0	0	0	0	0

distributions, both individually and together. The results indicate the following:

- Uniform flow distributions yielded $\eta_{reg} = 93.6\%$ (within 1% of the calculated disk effectiveness).
- Actual distorted gas-side flow distribution only decreased η_{reg} by 0.3%.
- With both air-side and gas-side flows distorted, the η_{reg} was reduced 10.6%.

Obviously the air-side flow path, while providing low pressure drop, was not providing the proper flow distribution required to maximize effectiveness. Two modifications to the cover have been modeled and tested and are shown in Figure 29 along with the baseline test. Mod I incorporated a ramp to redistribute the flow; the velocity profile shows a flattening of the profile in the hub region, but the resulting effectiveness was 13% below the uniform flow condition. Mod II blocked the top entry to the cover, and a second entry port was provided in the disk rim region. The resulting flat velocity profile restored effectiveness to within 1% of the uniform flow condition but at the expense of increased pressure drop (from 0.5% to 1.5%). Flow distribution testing of additional modifications will be continued to evaluate methods to reduce the pressure drop penalty and retain the design effectiveness of the disk. The engine regenerator cover will be reworked to optimize airflow distribution for engine performance testing.

Ceramic Exhaust Duct/Regenerator Seal Platform

Casting and machining was completed on the first of the single-piece ceramic (lithium aluminum silicate) exhaust duct/seal platform, as shown in Figure 30. Since the exhaust duct experiences the full ΔP of the engine operating pressure ratio, a test rig was developed to evaluate the stress/strain characteristics of the part when exposed at engine operating pressures. A cross-sectional view of this test rig is shown in Figure 31. Test instrumentation included pressure drop across the bulkhead, deflec-

tions at 27 locations, and strain gages on the bulkhead. In addition, "stresscoat" paint was applied to the first test piece to determine if there were high stress regions in locations other than those predicted by the finite element stress model. Figure 32 is a photograph of the bulkhead static test.

Figure 33 is a cutaway view of the ceramic exhaust duct showing a comparison of the predicted and measured deflection of part S/N 6 when loaded to maximum power conditions. Measured deflections were within allowable values for engine assembly/operation, and the maximum strain gage readings (see Figure 34) indicated stress levels in agreement with those predicted by the stress model. In addition to the deflection testing, each part undergoes X-ray and FPI inspection to identify any surface and interior defects of the part. Two pieces (S/N 8 and S/N 9) have completed qualification testing for use in the engine.

Regenerator Disk/Seal Performance

The first regenerator disk/seal set, fabricated by Harrison Radiator Division, was received in early April, and qualification testing on the leaf leakage rig and hot regenerator rig was initiated. Earlier testing of prototype design hardware had established the potential for reduced low-power (idle) seal leakage through use of modified seal

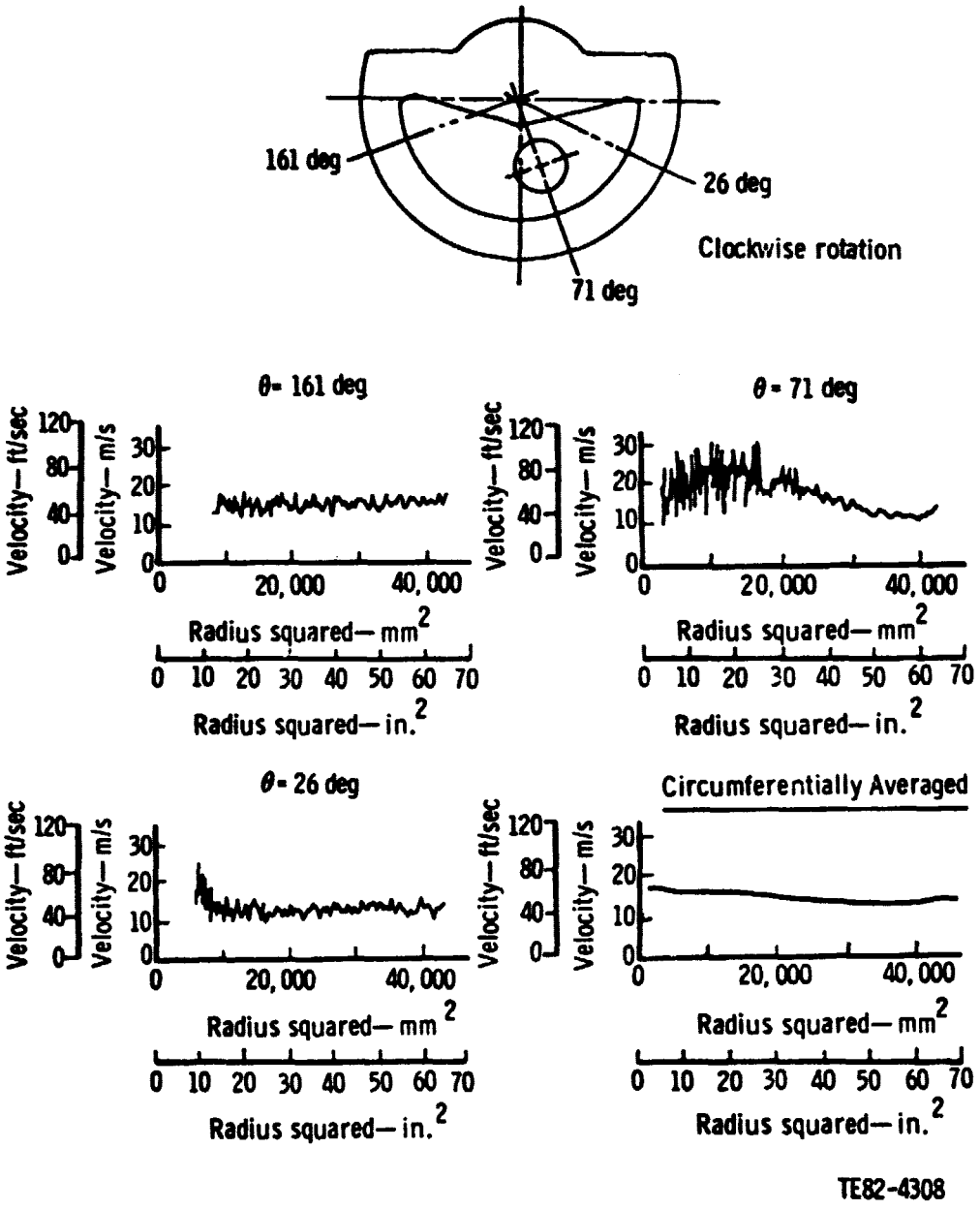

Figure 27. Regenerator measured gas-side cold flow distributions at maximum power condition.

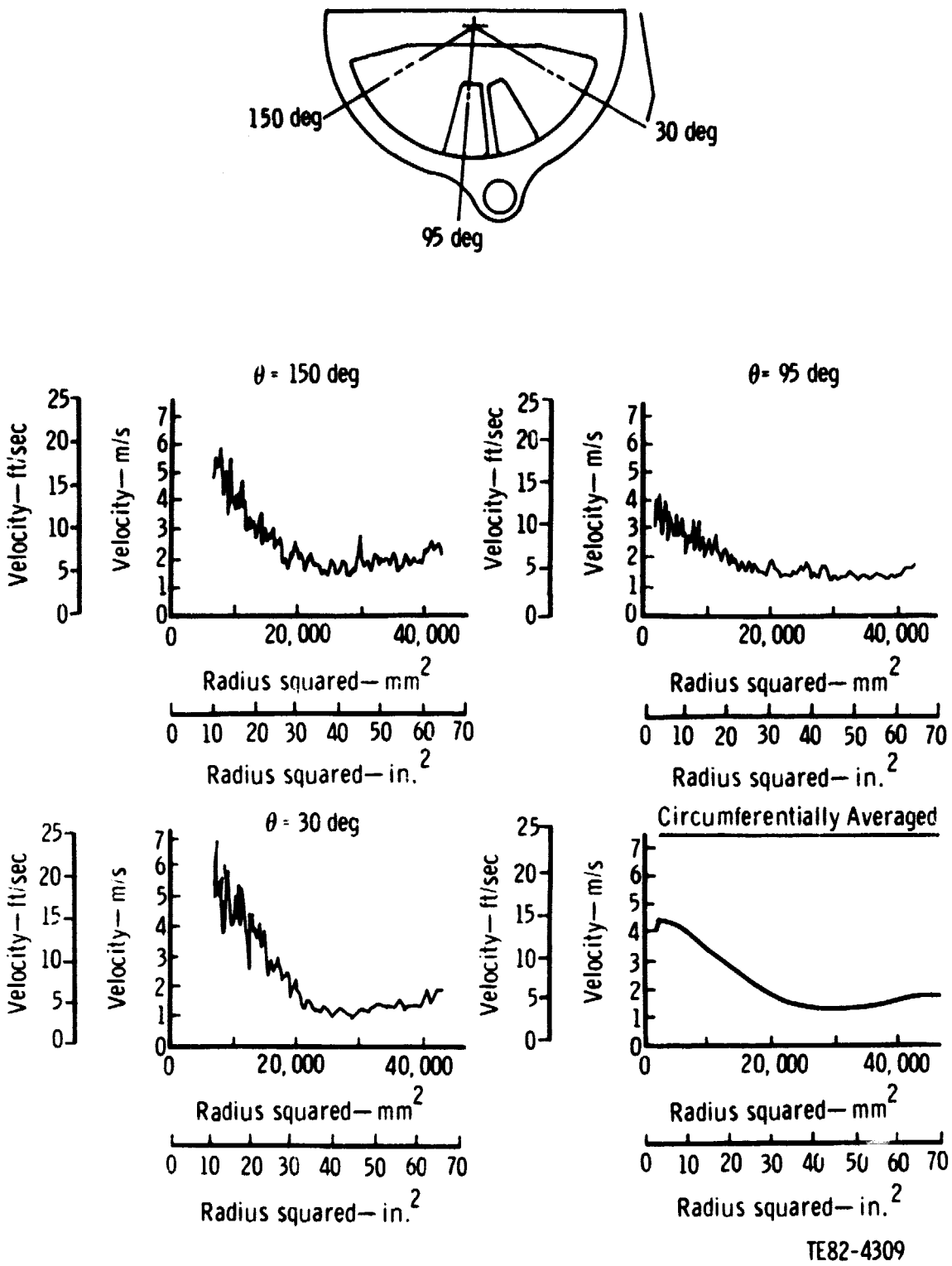

Figure 28. Regenerator measured air-side cold flow distribution at maximum power condition.

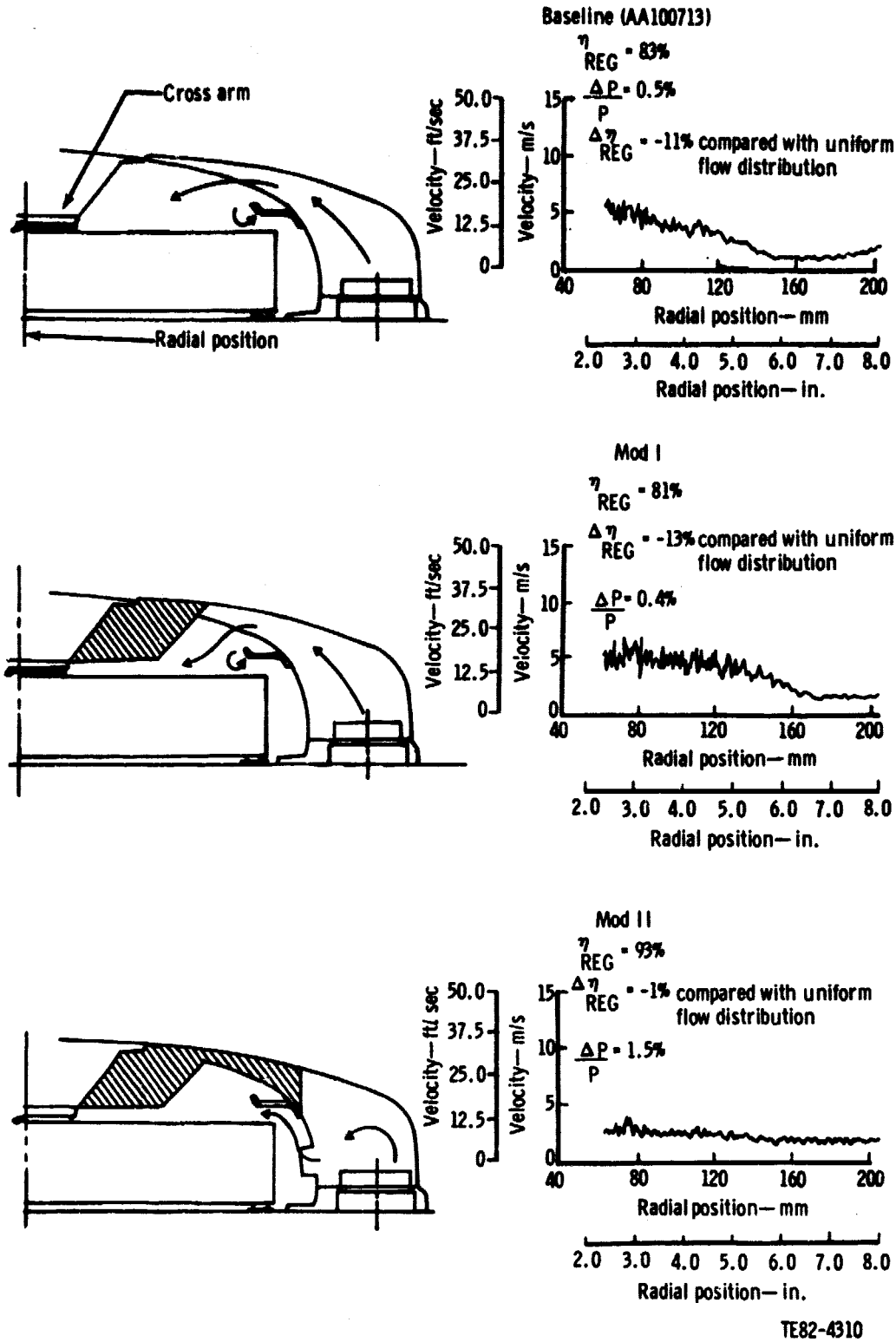

Figure 29. Regenerator air-side flow distribution testing.

crossarm grooving to maximize seal clamping forces. As a result, two outboard seal designs were fabricated for the engine; one with nominal clamping forces, and the second with maximized clamping. These are shown in Figure 35.

The test rigs were reworked to accept engine hardware and the initial testing "as received" resulted in unacceptably high system leakage, as shown in Figure 36. A series of minor changes to eliminate rig/seal interference and to reduce the rim/crossarm leakage of the inboard seal resulted in system leakage levels of 9%-10% (line B in Figure 36). Cold flow testing of the seals on the leaf leakage rig indicated significant leakage from the leaf joint areas—particularly at the corner miter joints. A modification to the seal leaf was made to add an O-ring backup under the leaf to ensure contact with the sealing surface on assembly and as compressor discharge pressure (CDP) is applied. The region between the O-ring and seal leaf was vented to CDP to ensure that the leaf was still the primary sealing member. The resulting leaf leakage, shown in Figure 37, illustrates the significant reduction in air leakage rates. A high-temperature (232°C [450°F]) silicone O-ring was installed around the perimeter of the outboard seal (with local venting openings); because of the high operating environment of the inboard seal, short (25 mm [1 in.]) segments of silicone O-ring were attached only at the corner miter joints and at the center of the crossarm. CDP cooling air in these regions reduces the temperatures locally to permit use of

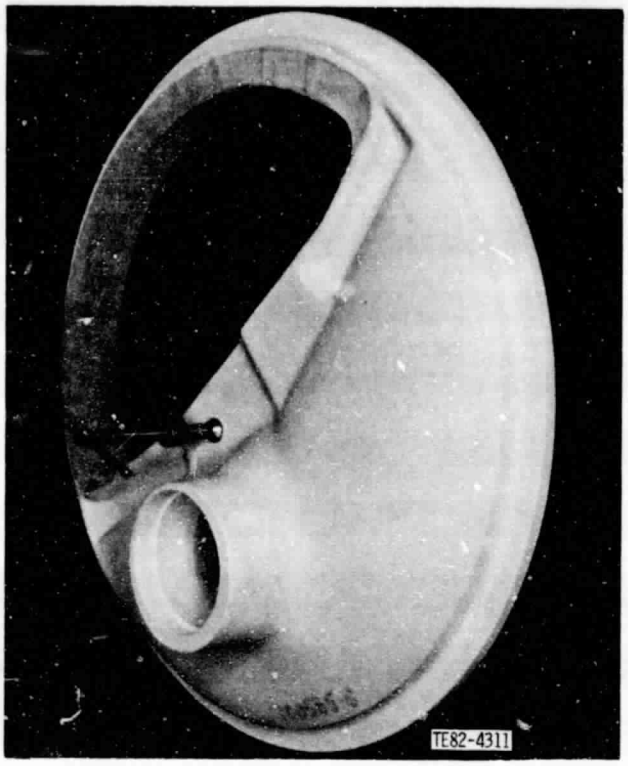

Figure 30. Ceramic exhaust duct/seal platform.

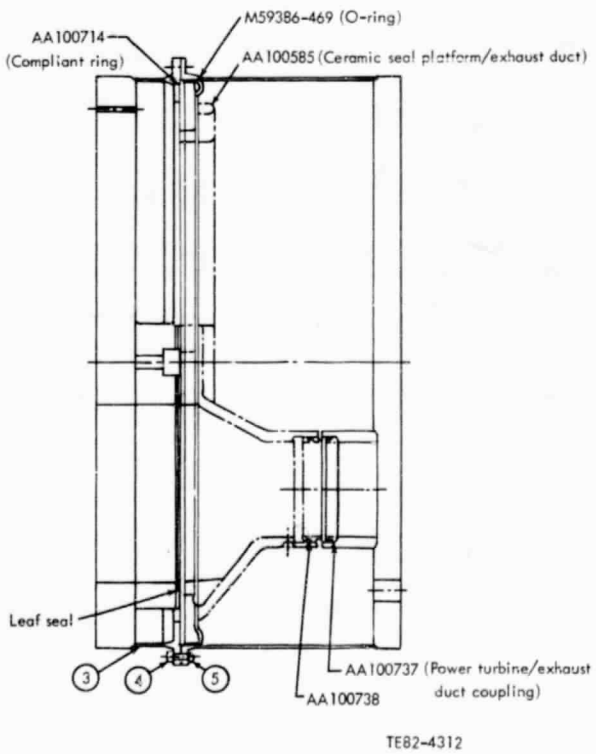

Figure 31. Ceramic exhaust duct/seal platform pressure test rig.

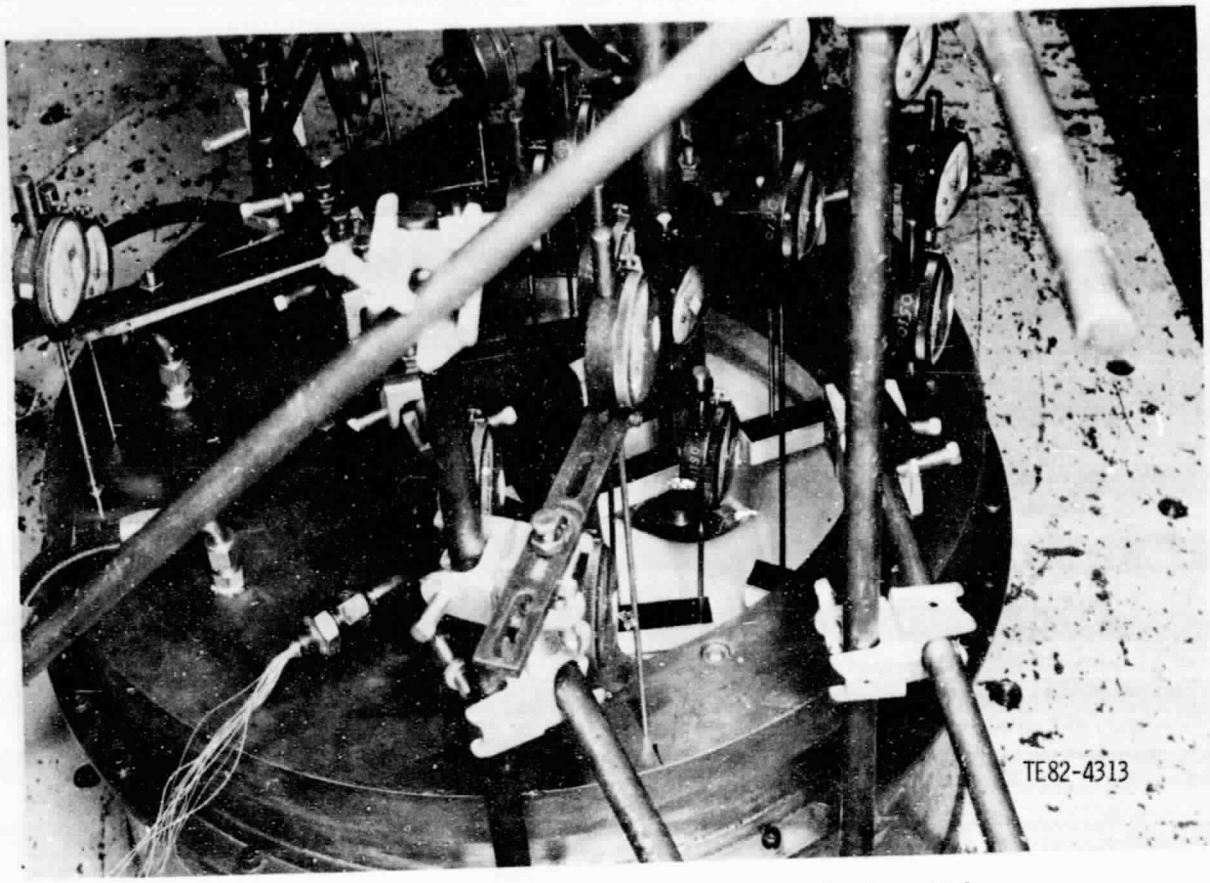

Figure 32. Exhaust duct/seal platform static stress test.

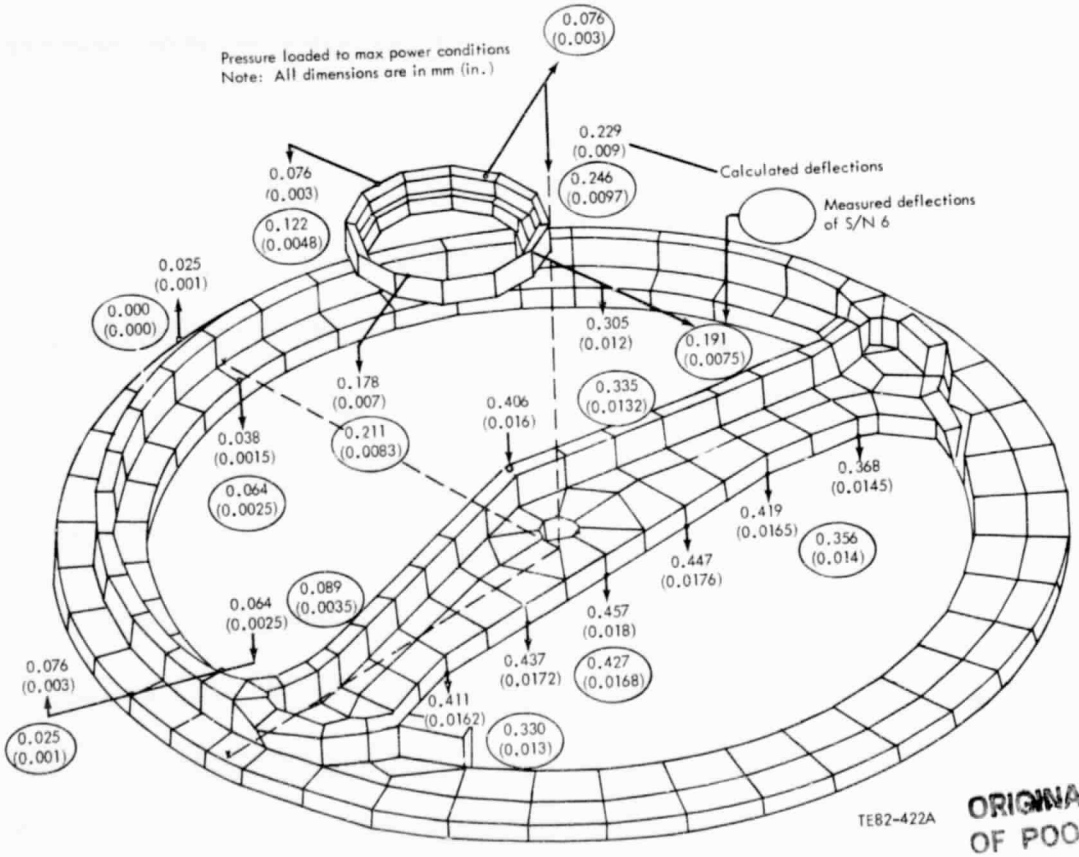

Figure 33. Deflection test results of ceramic regenerator seal platform.

the O-ring; this was verified with subsequent hot rig tests.

Both inboard and outboard seals with the O-ring backup were tested on the engine seal set and the alternate seal set. Data for the alternate seal set in this configuration are shown in Figure 36 (line C). Also shown is the same configuration tested with no inboard seal hub cooling air (line D). Reducing cooling air improves measured effectiveness but at the expense of increased leakage and, in the case of the O-ring backup, the decomposition of the O-ring at the center of the crossarm.

Subsequent hot rig testing of the alternate seal set was conducted to investigate an alternate to the O-ring backup at the inboard seal leaf joints. Helper springs were fabricated from 0.2 mm (0.008 in.) thick L605 and installed at each joint to aid leaf contact, and the data of line E in Figure 36 indicated performance very similar to the O-ring backup.

Additional testing of the alternate seal set provided data on build clearance requirements of the seals. The curves on Figure 38 indicate an installed seal clearance of 0.6 mm (0.025 in.) provides both improved leakage characteristics and adequate running clearances.

Regenerator drive torque and effectiveness for the two sets of seals are shown in Figure 39. The high clamping crossarm of the BU1 seal significantly increases the drive torque requirements. At the low regenerator speeds this represents approximately 0.45 kW (0.6 hp) at maximum power. More than 25 hr of hot rig test time has been accumulated with this high clamping seal without measurable deterioration in the seal wear surface or the disk.

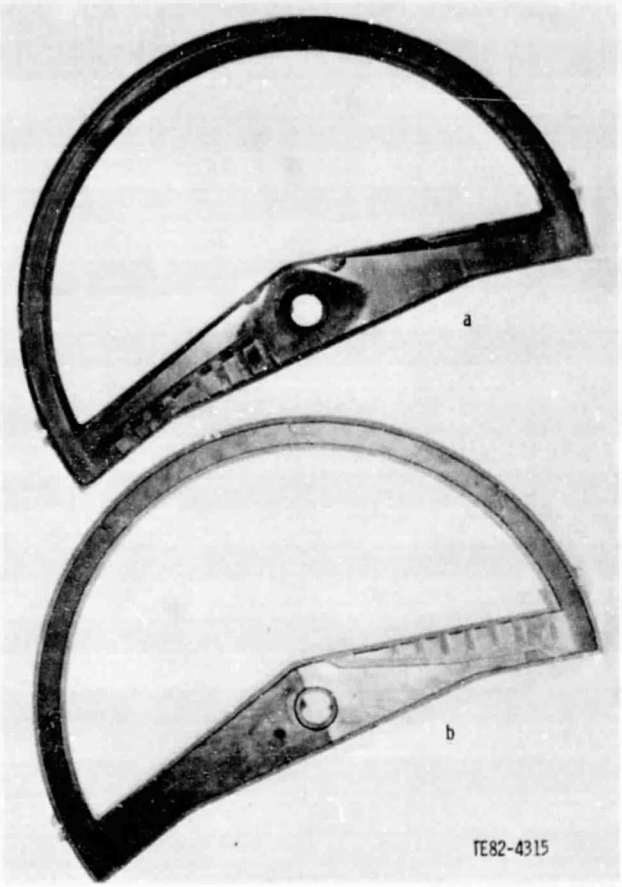

Figure 35. Regenerator outboard seals with (a) nominal clamping force and (b) maximum clamping force.

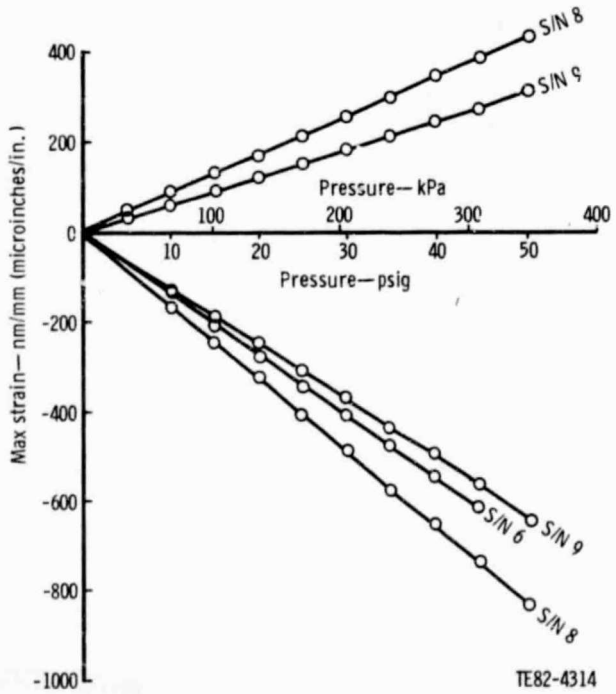

Figure 34. Proof testing of ceramic exhaust duct/seal platform.

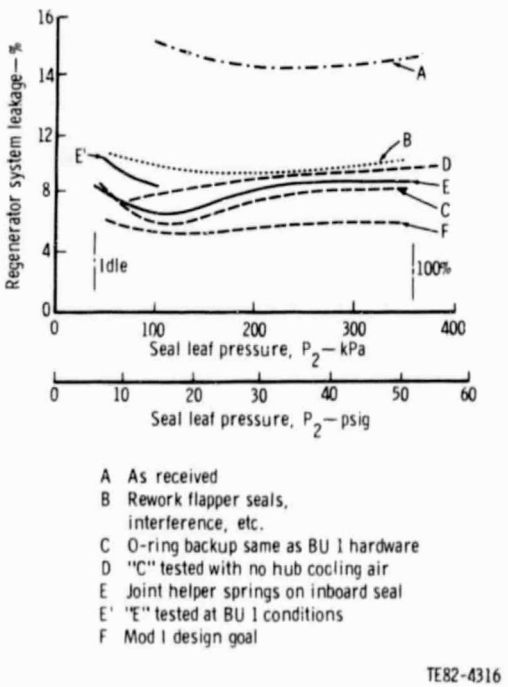

Figure 36. Development of alternate seals for BU1.

First Engine Build

The first engine build of the AGT 100 will be used to evaluate starting characteristics and low speed operation at reduced temperatures. The regenerator system hardware selection reflected these operating goals by providing reduced low-power leakage with the high clamping seal. The inboard seal incorporated the O-ring backup at the miter joints with full cooling airflow and the full perimeter O-ring backing of the outboard seal. The seal assembly clearance was adjusted to 0.6 mm (0.025 in.) with an outboard seal leaf height of 3.2 mm (0.125 in.).

The estimated regenerator system leakage and effectiveness are shown in Figures 40 and 41. The solid line on the leakage curve represents leakage levels at the Mod I design operating conditions; on the first build it is estimated that the engine will operate at lower temperatures at conditions more closely estimated by the free shaft configuration values shown. The effectiveness values shown for the engine build reflect the correction for differences in rig-to-engine disk blockages that reduce rig effectiveness levels.

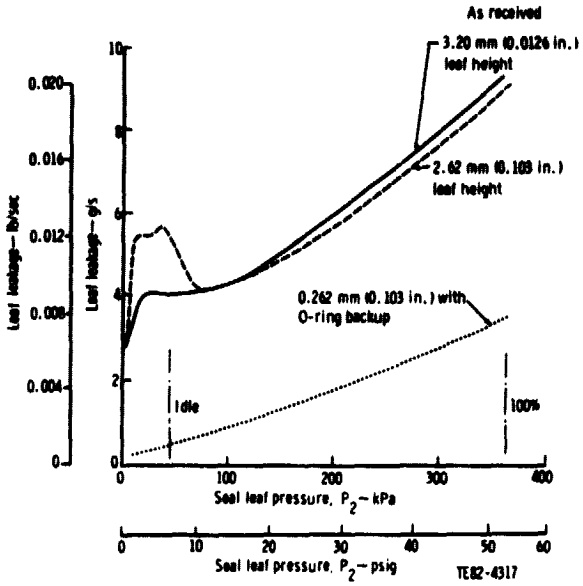

Figure 37. Outboard seal leaf leakage for BU1.

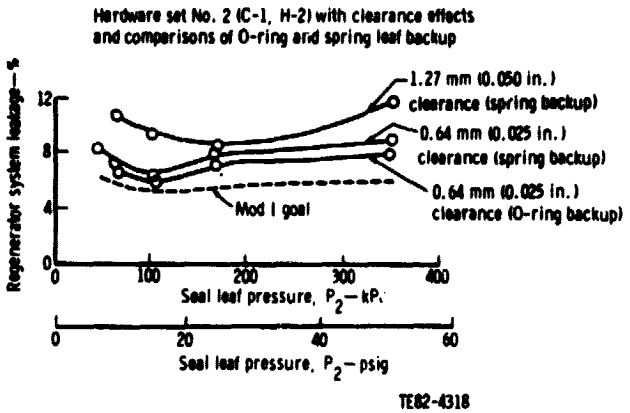

Figure 38. Comparative results of regenerator leakage testing.

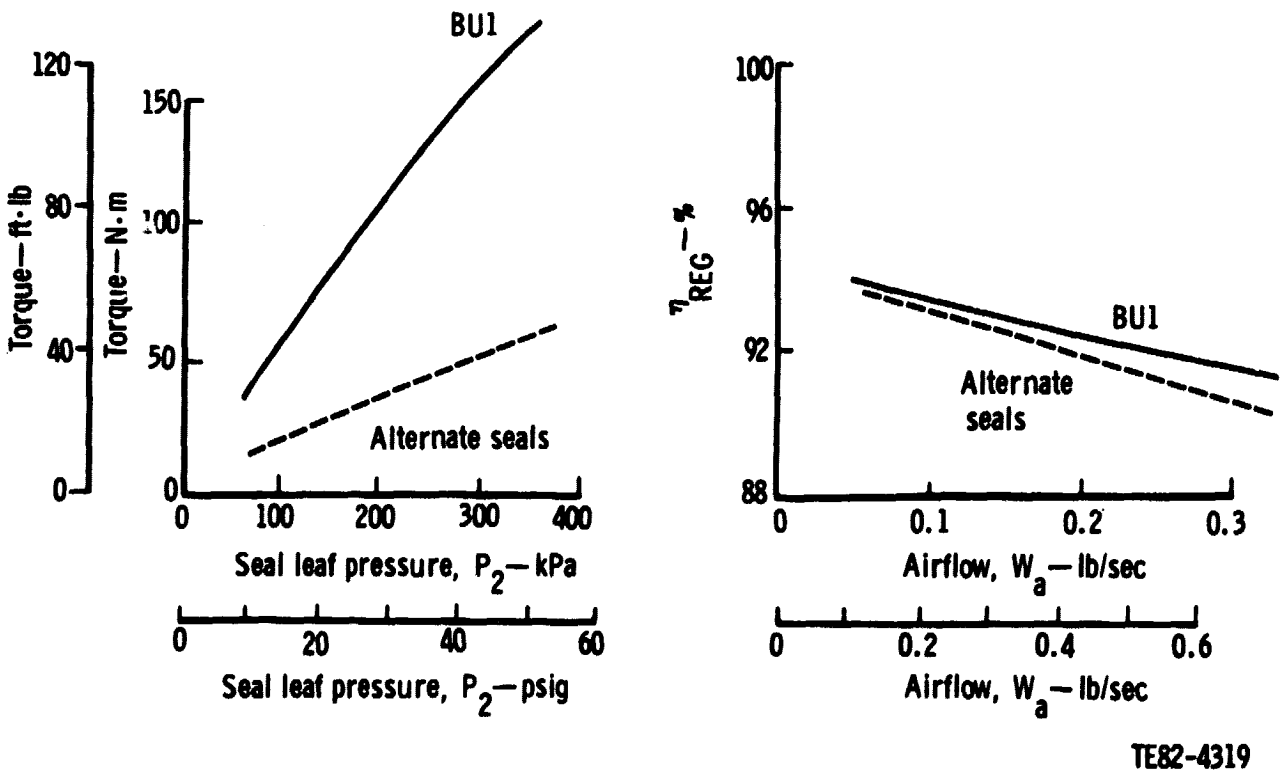

Figure 39. Regenerator drive torque and effectiveness for BU1 and alternate seal set.

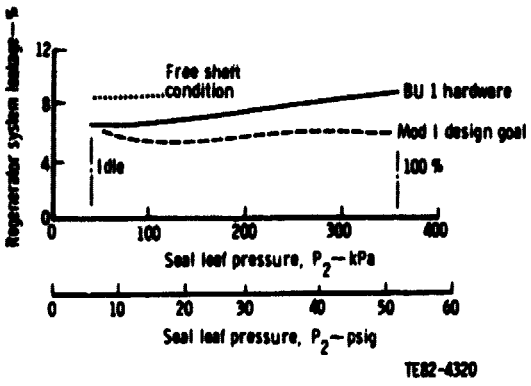

Figure 40. Regenerator system leakage for BU1.

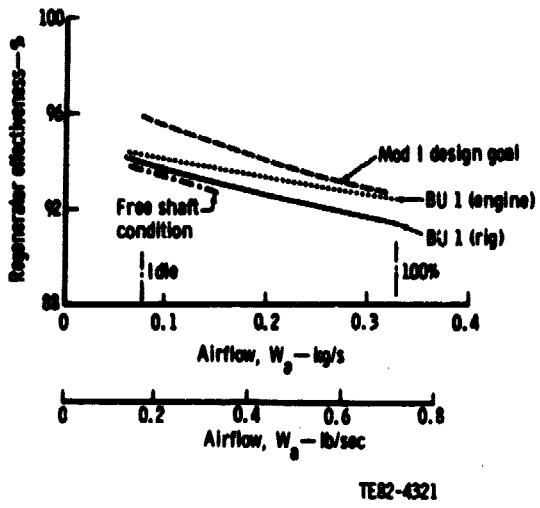

Figure 41. Regenerator effectiveness for BU1.

8.1 Structures

Combustion Case Assembly

A pressure proof test of the combustor case, inner gear case, and intermediate gear case was conducted. Together with the regenerator housing, these components form a pressure vessel that is the base structural load-carrying path through the engine. The regenerator housing was pressure tested separately and therefore was not included in this test.

The overall objective of the test was to subject the parts to the maximum pressure they would experience during engine operation. The specific test objectives included measuring the following:

- combustor case stress and deflection
- seal leakage
- inner gear case stress and deflection
- compressor shroud deflection

The overall test setup is shown in Figure 42. The combustor housing, inner gear case, and intermediate gear case are bolted together with all of the associated engine seals and gaskets to form a pressure tight structure. The rear flange of the combustor housing is bolted to a flat plate, which in turn is bolted to the test cell bed plate. The dial indicators, indicator frame, and strain gage measuring equipment are also shown in the figure. The dial indicators measure the inner gear case bearing pocket deflection and slope and compressor shroud deflection.

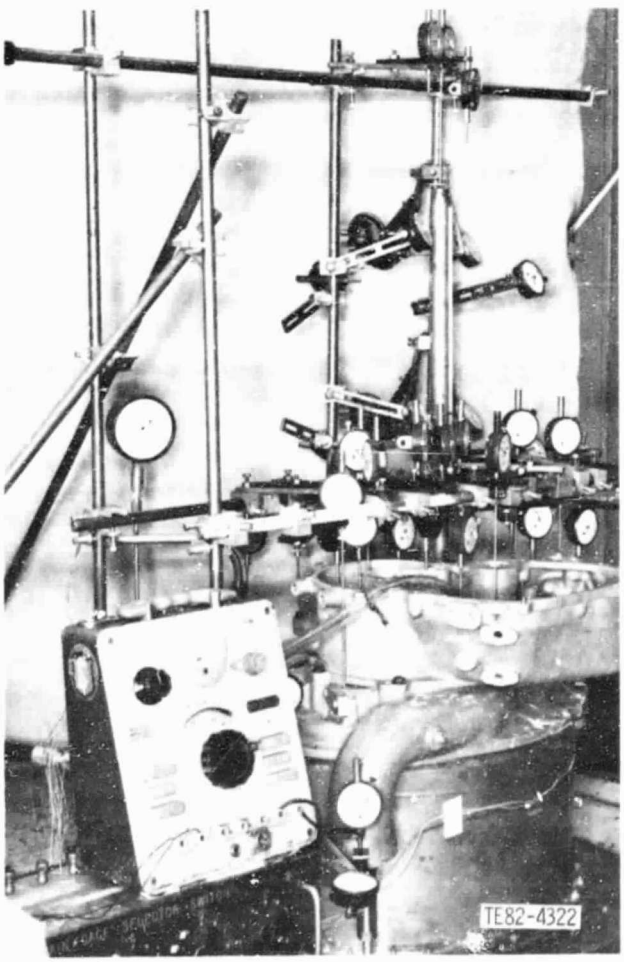

Figure 42. Combustor case/inner gear case pressure test.

The test was conducted in two steps. The first step identified the maximum stress area for location of strain gages. This was done by applying a brittle lacquer stress coat to the combustion case and inner gear case and applying 50% of maximum test pressure. The crack pattern in the stress coat located the maximum stress points. Figure 43 shows the maximum stress location in the combustor housing end wall (strain gages 31 and 32), and Figure 44 shows the maximum stress location in the inner gear case (strain gases 3 and 4). The stress plots for these locations are shown in Figure 45. A total of 41 strain gages were installed. The second step of the test was conducted with strain gages attached and dial indicators installed. Pressure was applied to the combustion case in stepped increments up to the maximum pressure of 482.6 kPa (70 psig), which is 100% of maximum engine operating pressure.

The maximum measured combustor housing stress was 372 MPa (54 ksi). Figure 46 is a comparison of measured

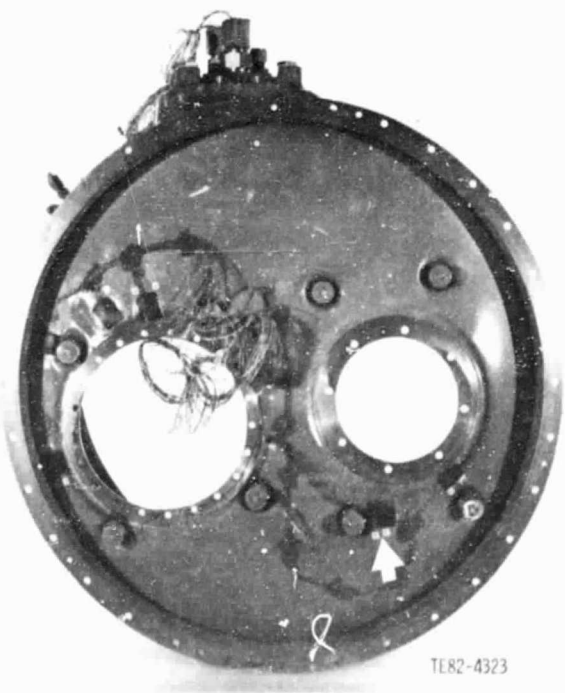

Figure 43. Combustor case strain gage location.

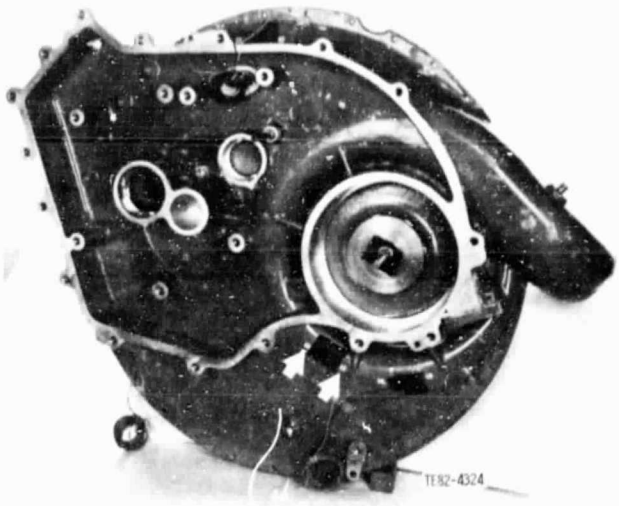

Figure 44. Inner gear case strain gage location.

and calculated stress in the combustor housing. In general, the measured stresses are significantly lower than the calculated values. The discrepancy can be explained by the differences between the computer model geometry definition, boundary conditions, and temperature gradient. The computer model assumed full fixity at interfaces between combustor case and inner gear case and included stress due to thermal gradients. The proof test was run at room temperature, and the spring rate of the actual parts determined the actual fixity at the interfaces. Since these stresses are all below the stress level of 0.1% creep in 1000 hr at engine operating temperatures, the parts met the design criteria.

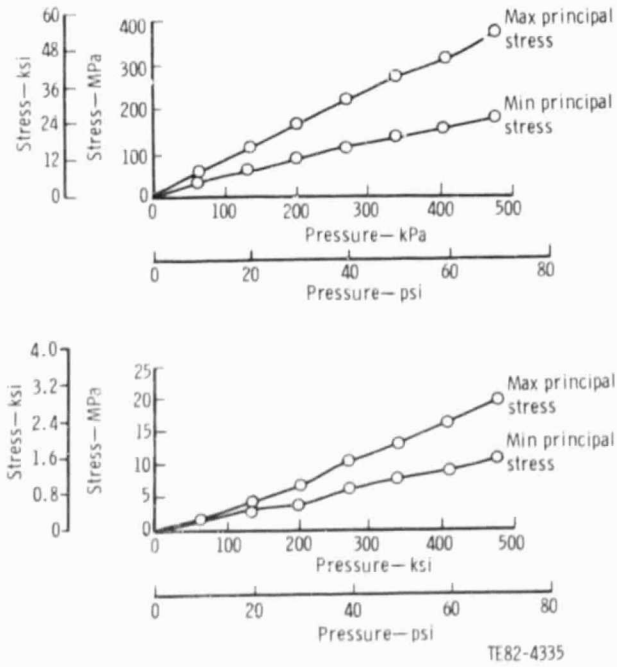

Figure 45. Stress and maximum stress locations for combustor case and inner gear case.

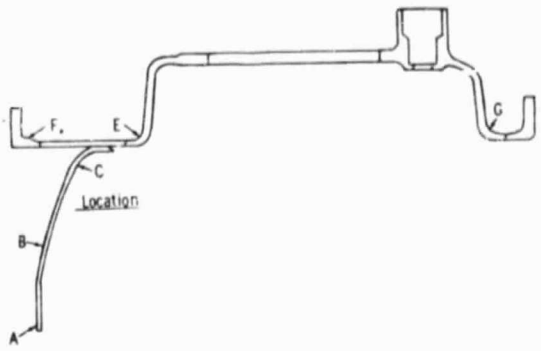

Stress condition

	Max power calculated		Max power measured	
	MPa	(ksi)	MPa	(ksi)
A	427.5	(62)	372.3	(54)
B	176.5	(25.6)	114.5	(16.6)
C	289.9	(42)	259.9	(32.7)
E	186.6	(27)	76.5	(11.1)
F	44.8	(6.5)	26.9	(3.0)
G	108.9	(15.8)	49.6	(7.2)
Case hoop	71.7	(10.4)	51.7	(7.5)

TE82-4325

Figure 46. Combustor housing stress summary.

The interface seal leakage between the combustor case and inner gear case was 0.0005 kg/s (0.0011 lb/sec) at the maximum 482.6 kPa (70 psig) pressure condition. This is 0.15% of engine flow at the maximum power condition, which was considered an acceptable level.

The maximum stress in the inner gear case was 20.0 MPa (2.9 ksi) and is located on the compressor scroll. The maximum stress was calculated from rectangular strain gage rosettes (gages 3 and 4), shown in Figure 44. The inner gear case material is AA 355-T6 aluminum, which has a yield strength of 89.6 MPa (13 ksi) at 204°C (400°F), the maximum operating temperature condition.

The maximum deflection in the intermediate gear case was 0.305 mm (0.012 in.) located at the output shaft bearing pocket (indicator No. 28) and an associated bearing pocket slope of 0.0008 mm/mm (0.0008 in./in.) at 482.6 kPa (70 psig), as shown in Figure 47 (indicator Nos. 24 and 25). The stress in this area of the case was less than 12.4 MPa (1.8 ksi). The differential deflection between the inner gear case and the intermediate gear case at this same location (output shaft bearing pocket) was 0.183 mm (0.0072 in.) at maximum test pressure. All shafts have sufficient end play to accommodate this reduction in clearance due to pressure loading.

The axial deflection at the inducer of the impeller shroud, which is integral with the inner gear case casting, varied circumferentially between 0.127 and 0.305 mm (0.005 and 0.012 in.) at 482.6 kPa (70 psig). This deflection should not present any problem in engine operation

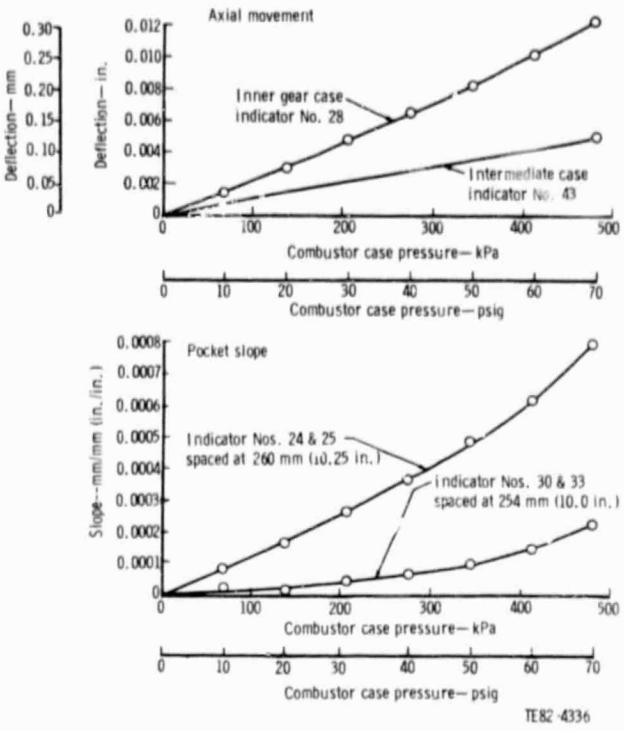

Figure 47. Deflection measurements of inner gear case.

since the impeller bearing pocket and the shroud are essentially part of the same structure, and therefore the impeller-to-shroud clearance will not be affected by the pressure load. The measured deflection is also higher than will be experienced in engine operation since in the test the entire shroud area was pressurized to 482.6 kPa (70 psig). In the engine the shroud pressure will vary from inlet pressure to compressor discharge pressure.

8.2 Gearbox and Power Transfer

The harmonic drive reduction gearbox was tested during this reporting period. The following testing schedule was designed to test the basic operation of the unit first at no load conditions and then at progressively increasing load conditions to the design point:

1. 1 hr – no load
2. tear down and inspect
3. 2 hr – 11.9 N·m (105 lb-in.) load
4. tear down and inspect
5. 2 hr – 23.7 N·m (210 lb-in.) load
6. tear down and inspect
7. 2 hr – 35.6 N·m (315 lb-in.) load
8. tear down and inspect
9. 3 hr – 35.6 N·m (315 lb-in.) load

10 hr total at 3000 rpm input

While running the no-load portion of the schedule, a flex gear drive tang failed. Upon inspection some indication of wear was noticed on the sides of the output shaft teeth. The unit was reassembled and the test continued. At approximately 45 minutes into the schedule the flex gear failed, locking the unit. This unit is shown in Figure 48.

Analysis of the failed unit revealed more wear on the sides of the output shaft teeth and cracking of several

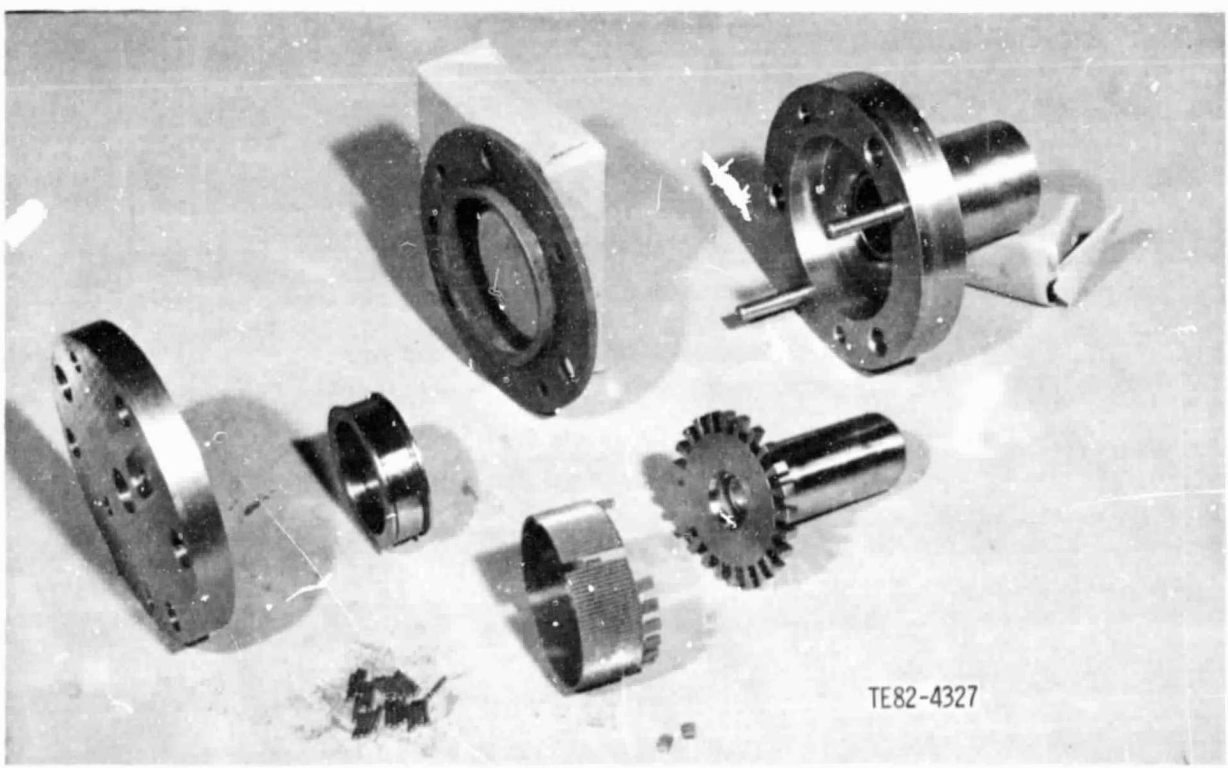

Figure 48. Failed harmonic drive unit.

flex gear tangs at the root filler. At that time it was thought that the radial flexing of the flex gear produced the wear due to interference with the output shaft. The geometry of the rubbing surfaces was such that a sharp edge was presented to the output shaft, causing wear. The output shaft slots were widened and the geometry was changed to be parallel to the sides of the drive tangs, eliminating any cutting action.

At this time, tc it was found that the flexing of the flex gear due to tl cam was causing the flex gear tangs to advance and retreat circumferentially with respect to the output shaft teeth. This relative motion created an interference, causing distress in the flex gear tangs. The rework eliminated this interference.

Testing of the modified unit began with a test of the fatigue life of the flex gear. This test was run in the harmonic drive units without the output shaft, thereby inducing no load on the tangs. The only loading of the flex gear was the twice-per-revolution flexing caused by the cam.

The flex gear successfully completed 6.6×10^6 cycles of this testing with no crack indications. The reworked output shaft was then installed and the testing schedule restarted. Fifteen minutes into the 11.9 N·m (105 lb-in.) portion of the test, the second flex gear failed.

As a result of this second failure and inconclusive results from a study of a modified harmonic drive, all effort was directed toward a new reduction gearbox assembly. The results of this effort are shown in Figures 49 and 50.

The new gearbox is a planocentric unit. The input shaft drives a counterbalanced cam, which rides in 28 needle rollers. This cam drives a 60-tooth external gear within a 62-tooth fixed internal gear, producing the required 30:1 reduction. Power is transmitted through a cross-keyed slider to the output shaft. Lubrication for the unit is taken directly from the oil pump. Testing of this unit will follow the same schedule as the original harmonic drive.

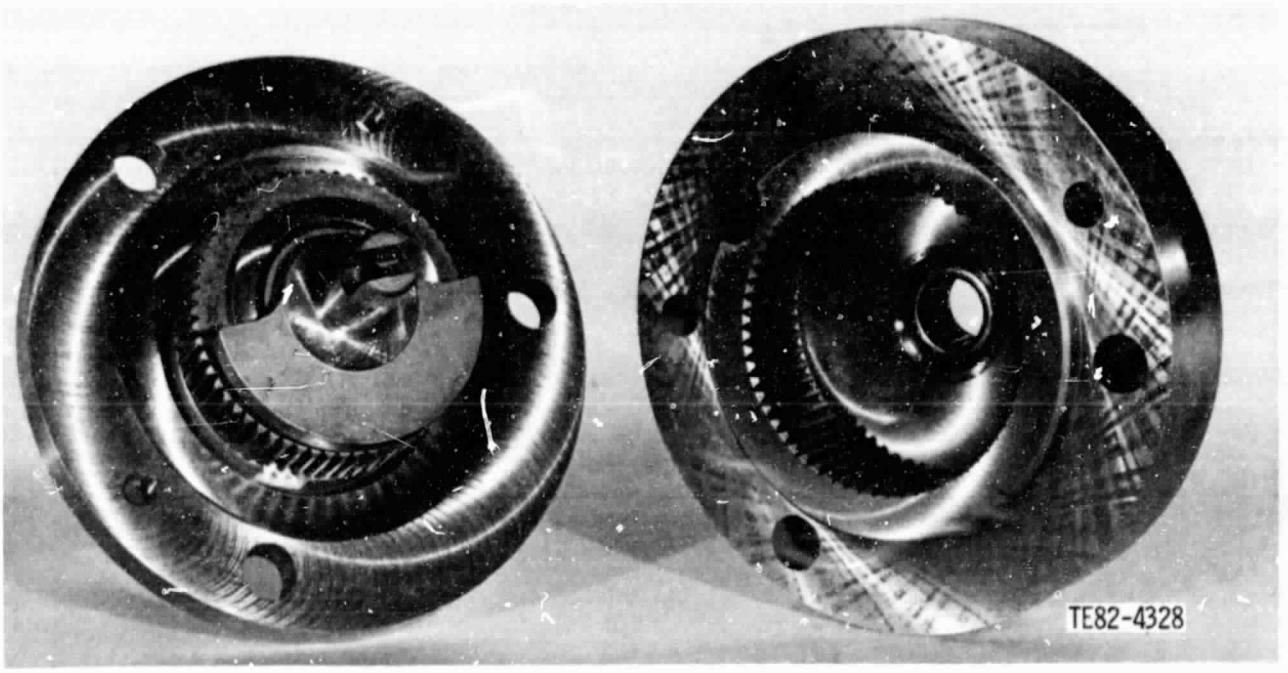

Figure 49. Regenerator drive gearbox—input side.

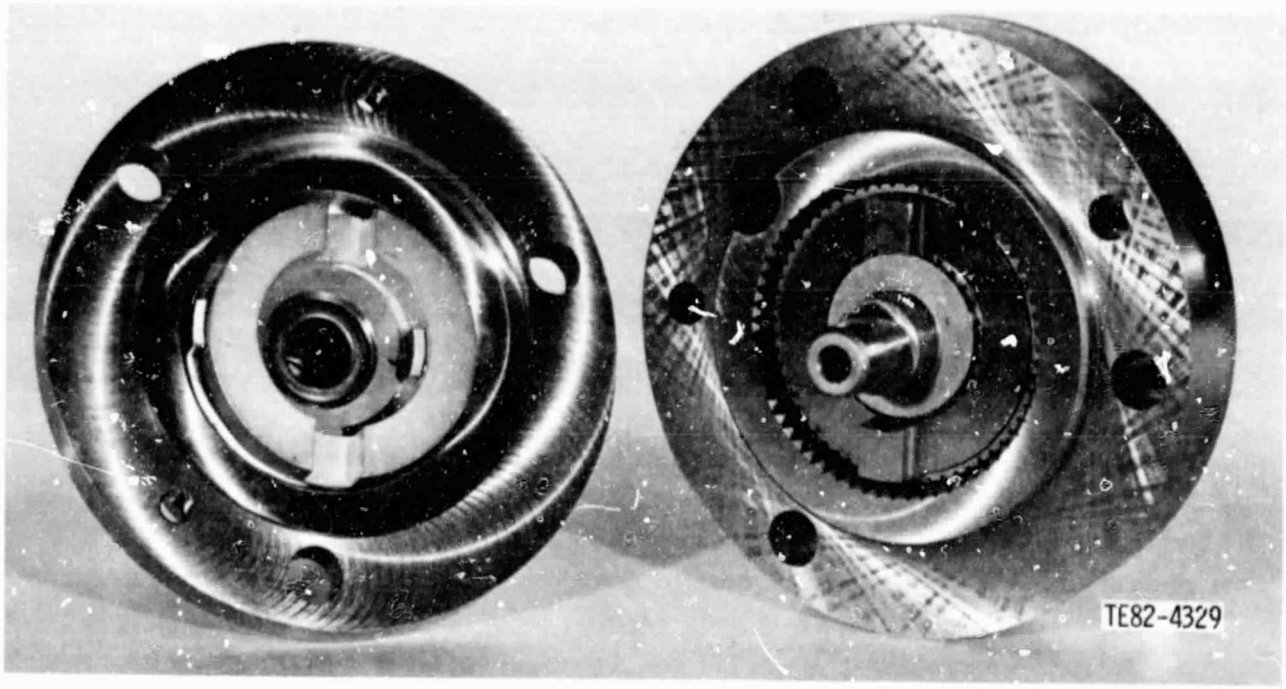

Figure 33. Regenerator drive gearbox—output side.

IX. Materials Development

9.1 Thermal Barrier Development

Within the present reference power-train design (RPD) there exists the need for several noncarbide ceramics. These materials are being developed in two parallel efforts. DDA is developing a zircon-based material, and the Carborundum Company (CBO) is addressing a mullite/cordierite composite material. Both of these materials have special low heat conduction characteristics and will be used primarily as thermal barrier structures intended to minimize heat loss from the gas path to the surrounding metallic support structures. The following subsections summarize the status of the respective development efforts.

Carborundum Effort

The mullite/cordierite under development at CBO is being produced by isopressing and sintering of sol-gel prepared powders. Initial work focused on establishing the proper composition to produce the best coefficient of thermal expansion (CTE) with alpha silicon carbide. Materials with the best CTE match have been found to contain approximately 59% mullite and 41% cordierite. Work during this period was directed at improving the strength of this composition.

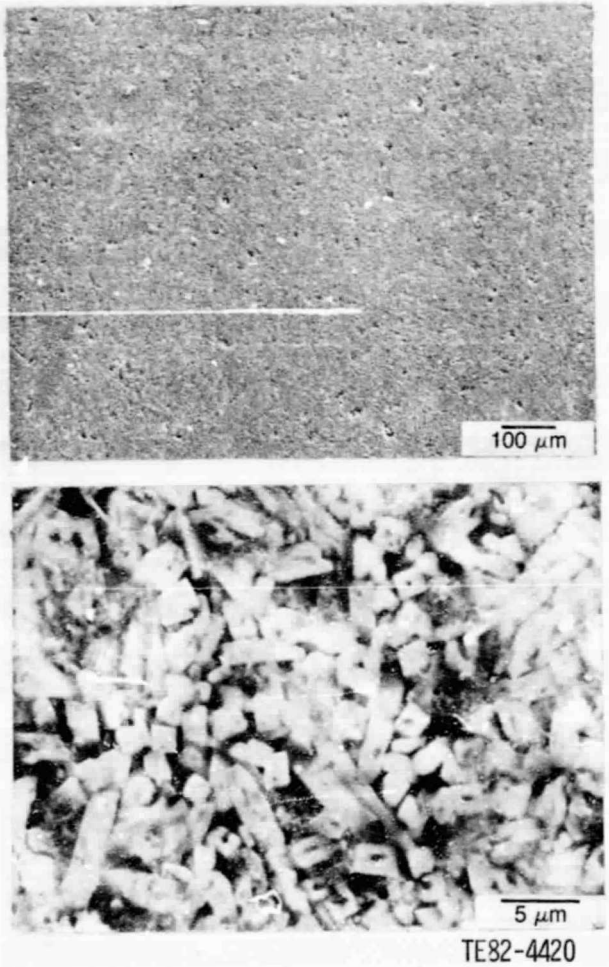

Figure 51. Microstructure of CBO mullite/cordierite.

Improved powder processing and firing techniques have helped to produce materials with reduced porosity. This improved material has been characterized to determine the microstructure, crystalline phases, and fracture strength (modulus of rupture).

Figure 51 illustrates the high degree of uniformity of the present composition. Experience has shown that the sol-gel derived powders yield a very fine grained microstructure. X-ray diffraction analysis showed that the material consists predominantly of mullite and cordierite with magnesium-aluminum spinel as a minor phase. The scanning electron microscope (SEM) photomicrograph shows that these phases are uniformly dispersed and consist of grains smaller than 5 μm in diameter. Standard water immersion techniques on this material showed that the material had negligible water absorption. Any porosity present would, therefore, be closed. Table IV lists the properties measured for this material. The strength level represents a significant improvement over earlier materials.

Table IV. Physical properties of CBO mullite.

Property	Results
Coefficient of thermal expansion	5.07×10^{-6}/°C at 1300°C (282×10^{-6}/°F at 2372°F)
Density	2.77 g/cm^3
Modulus of rupture (0.1 × 0.2mm X-section, third point loading)	118.7 MPa (17.21 ksi), s = 8.4 MPa (1.22 ksi) n = 12
Modulus of elasticity (sonic)	149,616 MPa (21,700 ksi)

DDA Effort

Previous work has demonstrated that zircon-based materials can be readily fabricated. To date work has indicated that materials produced from zircon possess suitable strength and expansion characteristics. Work during this period centered on (1) microstructure improvement and (2) strength and thermal expansion characterization.

Early materials had an apparent pore fraction of approximately 0.18. Information obtained from recent literature indicated that sintering aids could be introduced to enhance the sinterability of zircon. As a result, material compositions were established that displayed negligible apparent pore fractions.

These materials have been produced using classical isopressing techniques. Figure 52 illustrates the microstructure of the best material. Figure 53 shows the respective thermal expansion behavior. The overall ex-

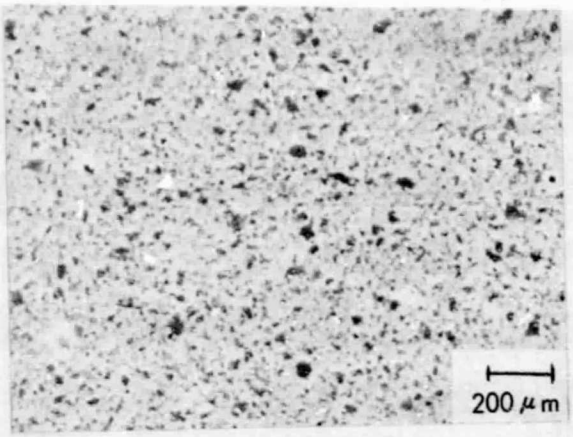

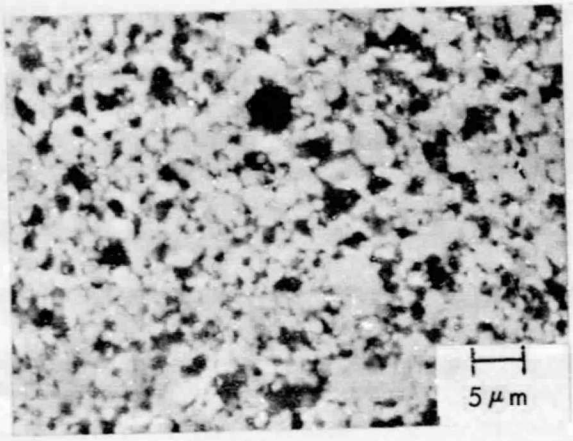

Strength to date = 128.5 MPa (18.64 ksi),
std dev = 1.91, n = 7
Modulus of elasticity = 174.8 MPa (25.35 ksi)
Poisson's Ratio = 0.42
CTE = 4.61×10^{-6}/°C at 1000°C
(2.56×10^{-6}/°F at 1832°F)

TE82-4421

Figure 52. Microstructure for DDA zircon.

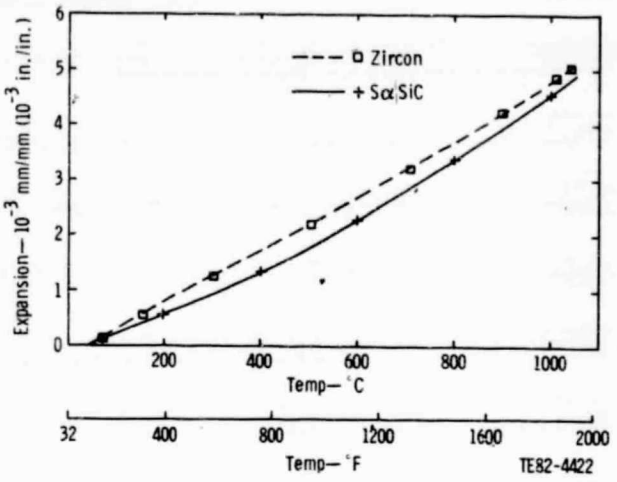

Figure 53. Thermal expansion behavior of DDA zircon.

pansion behavior is a suitable expansion match for silicon carbide. Table V lists the phase character of this material along with available properties.

Table V. Phase character and properties for DDA zircon.

Crystalline phases by (X.R.D.A.)	Zircon, mullite, and cristobalite
Modulus of elasticity at room temp	204,912 MPa (29,720 ksi)
Poisson ratio	0.256
Sample size	12 bars
MOR (room temperature, as fired)	167.5 MPa (24.29 ksi)
Standard deviation	30.4 MPa (4.412 ksi)

The strength was measured in four-point bending, with the outer span 38.1 mm (1.5 in.) and the inner span 19.1 mm (0.75 in.). All bars were a standard size of 3.175 mm × 6.35 mm × 50.8 mm (0.125 in. × 0.25 in. × 2 in.). Fracture originated predominantly from the surface. Typical fracture origins are shown in Figure 54. The strength observed for this generation of DDA zircon is the highest yet obtained and is superior to all other materials procured to date.

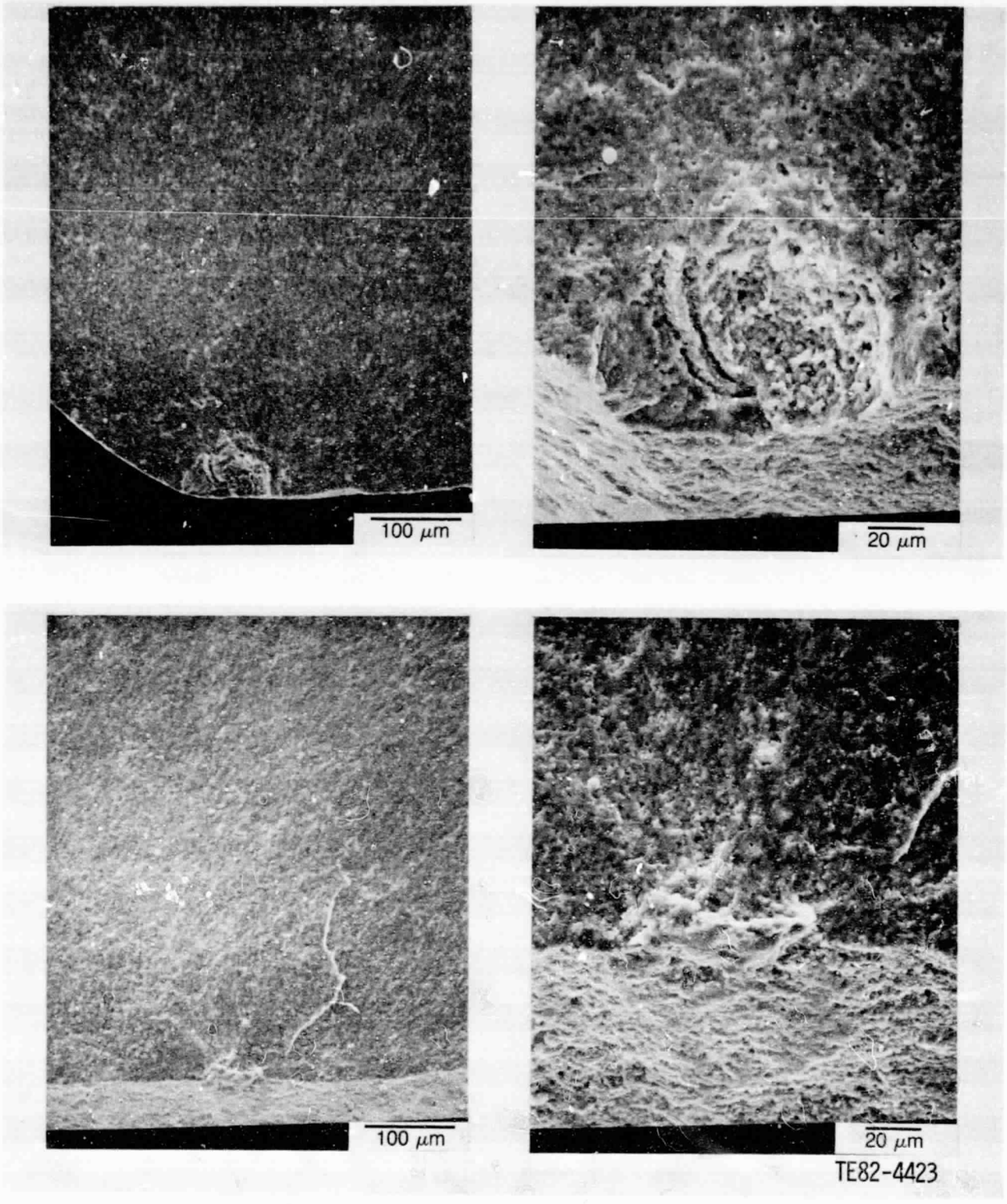

Figure 54. Fracture origins in DDH zircon.

9.2 Ceramic Component Development, Characterization, and Qualification

Work has centered on the fabrication, characterization, and qualification of silicon carbide and zirconia components. Work to date has included a ceramic combustor assembly, turbine vanes, and thermal insulators in the Mod I engine build.

Some components can be produced by available state-of-the-art techniques while others require developmental efforts. Those components produced by isopressing and green machining, such as the swirl plate and inner backplate, are state of the art. However, unique development efforts are needed for injection molded gasifier rotors and outer backplates, and also for the slip casting of scrolls and related components. Details of the characterization and qualification of state-of-the-art components and prototype components are contained in the following subsections.

Silicon Carbide Component Development

Gasifier Rotor

This component is being fabricated from injection molded sintered alpha silicon carbide. Fabrication variables have been systematically controlled to help yield optimum spin test results. Work during this period focused on characterization of material strength in various regions of the rotor. These measured strength results were then compared to requirements dictated by finite element analyses and correlated with actual spin test results.

One hundred prototype rotors were molded by the optimum molding procedures. Experiments have shown that sintering atmosphere and composition are most critical for producing high-quality rotors. Composition relates to the starting percentages of powder and flow-inducing plastic. Table VI illustrates the impact of sintering atmosphere and material composition on the processing yields of A and B quality prototype rotors. Based on the limited amount of data available, it appears that atmosphere 2, in conjunction with compositions 2 and 3, provides the highest yields of acceptable rotors.

Table VII summarizes the results of the overspeed-to-failure spin testing conducted on A and B quality prototype rotors. The burst speeds were used to generate a Weibull plot, as shown in Figure 55, and a Weibull modulus (m) of 7.25 was obtained. Using 7.25 for m and 97,000 rpm for the median spin burst speed, an approximation was made for the average strength of the rotor material. The results of this analysis showed that the material should have an equivalent MOR bar strength of 49.3 ksi. MOR tests for bars cut from actual rotors, listed in Table VIII, show that there is very good agreement between the predicted value of 49.3 ksi and the strength of the radial cut test bars. The strengths are considerably lower, however, for the axial cut bars.

The rotor shaft was redesigned to facilitate joining to the metal turbine shaft. The shaft outer diameter was enlarged to 14.0 mm (0.55 in.) to increase its strength in

Table VI. Processing yields* of A and B quality prototype rotors.

	Composition			Total
	1	2	3	
Atmosphere 1	0%	17%	–	13%
Atmosphere 2	0%	56%	83%	60%

*Yield is expressed as a percent and represents the number of acceptable parts divided by the total number of parts made.

Table VII. Burst speeds for prototype rotors.

Rotor S/N	Burst speed—rpm
438	106,000
439	97,600
445	82,000
475	92,000
476	107,500
477	111,500
404	98,500
424	94,000
437	96,000
472	98,000
Mean	98,300
Standard deviation	8,400

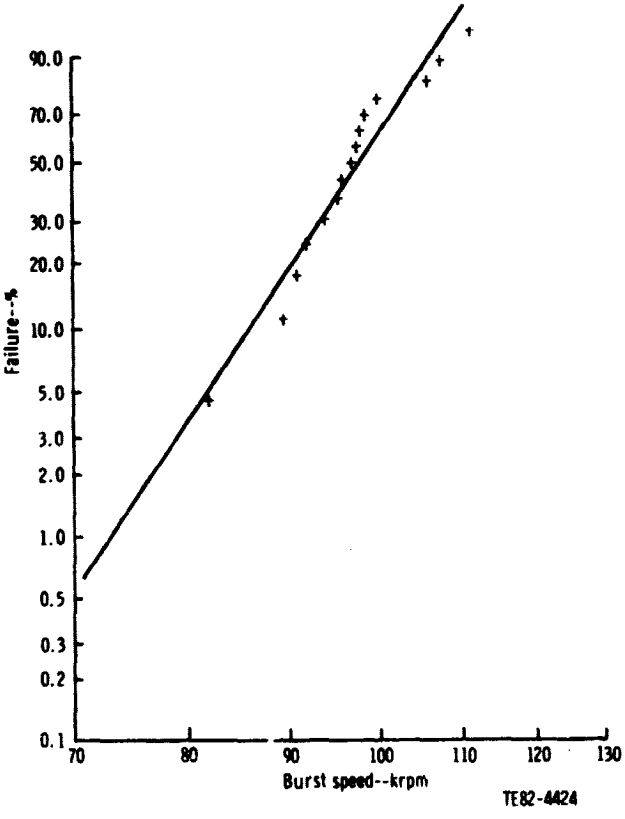

Figure 55. Weibull plot for burst testing of gasifier rotors.

Table VIII. MOR bar strength of prototype rotors.

Rotor No.	Density Rotor ρ	Density Bar ρ	Direction of cut	Strength —ksi	Range	Std Dev, σ	Composition	Atmosphere
432	3.14	3.12	Radial	$46.9\bar{x}_7$	32.0 → 58.5	9.1	2	2
433	3.13	3.08	Axial	$26.6\bar{x}_5$	19.0 → 30.0	4.4	2	2
463	3.08	3.09	Radial	$48.0\bar{x}_6$	41.1 → 63.9	8.6	2	1
493	3.07	3.00	Axial	$30.3\bar{x}_4$	24.1 → 35.7	5.2	1	1
482	3.12	3.04	Axial	$31.8\bar{x}_5$	23.1 → 46.5	8.8	2	2
484	3.12	3.07	Radial	$50.2\bar{x}_{11}$	36.6 → 70.7	11.2	2	2

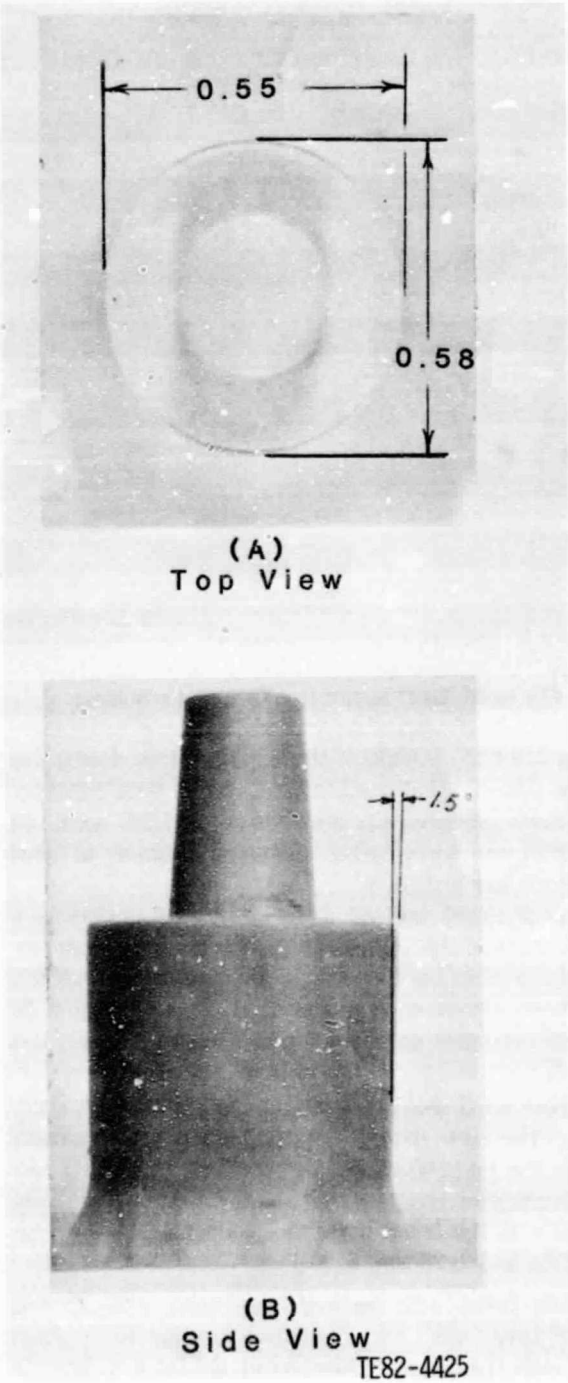

Figure 56. Rotor shaft modifications.

Table IX. Densities for gasifier rotors.

Rotor No.	Density— g/cm³
51	3.10
52	3.10
53	3.10
54	3.10
55*	3.09

*Spinnable

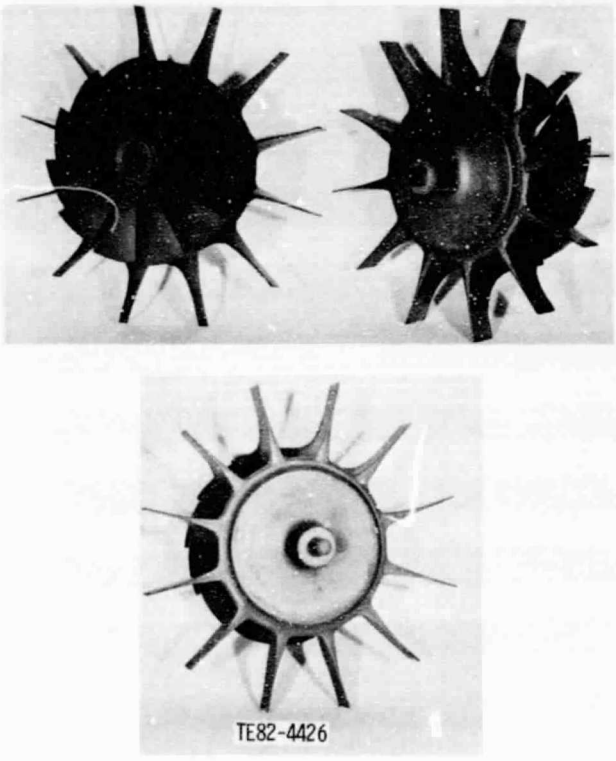

Figure 57. CBO gasifier rotors.

the event of whipping. The mold was also modified to incorporate a 1.5 deg reverse taper on the end of the shaft and to make it 0.76 mm (0.03 in.) out of round. Figure 56 illustrates the modifications made to the shaft. One hundred rotors have been molded from two compositions at various molding conditions.

Table IX lists density results for rotors molded with the new shaft geometry. Figure 57 shows rotors received

Table X. Combustor bodies received January through July 1982.

FX No.	Quality	Surface	MOR—MPa (ksi)	Std dev—MPa (ksi)	No of samples	Comments
			MOR qualification data			
30458	C	As fired	347.3 (50.37)	49.9 (7.24)	5	Not machined,
		Machined	401.2 (58.19)	72.9 (10.57)	5	has cracks
30459	B	As fired	317.0 (45.98)	56.1 (8.14)	5	Machined dilution
		Machined	316.8 (45.95)	48.3 (7.01)	5	and flame tube holders
30460	B+	–	– –	– –	–	–
30461	B	As fired	333.4 (48.36)	31.6 (4.59)	10	Received machined, two chips on i.d., oversize i.d. = 0.254 mm (0.010 in.)

Figure 58. Machined CBO combustor body.

during this period. Quality determinations and spin tests have yet to be made for the new design rotors.

Combustor Assembly

The combustor body is being produced from slip cast alpha silicon carbide. Work previous to this period has centered on prototype component development. During the latter part of 1981 a design was determined for this component to be used in the engine. Work during this period has included procurement, quality determination, and qualification for the new design. At CBO work has centered on improving the shrinkage reliability to meet blueprint specifications.

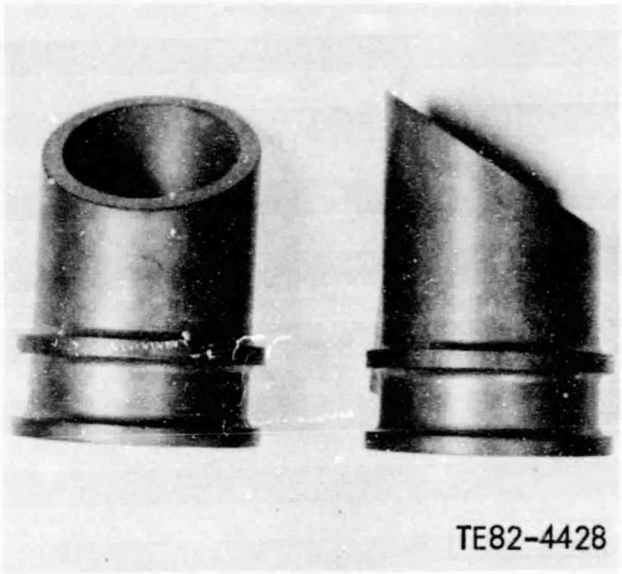

Figure 59. CBO combustor flame tube holders.

Four slip cast sintered alpha combustor bodies have been received this period. Table X lists information pertaining to these components. Combustor body FX30459 has been incorporated in the Mod I engine. Figure 58 shows the latest combustor body received during this period.

A new mold was produced for casting the combustor body. The new mold was designed to more closely match the material shrinkage behavior. In the first two combustors received the i.d. was oversized 0.75 mm (0.030 in.). The latest body received, 30461, was oversized by only 0.25 mm (0.010 in.).

Three flame tube holders have been received this period (see Figure 59). These were made from green machined sintered alpha silicon carbide. Table XI lists the NDE and quality status for these parts.

Two fully machined swirl plates were received this period. These components are made by green machining a rough shape followed by ultrasonic machining of the slots. The material is sintered alpha silicon carbide.

These two swirl plates were each assembled in a burner rig for proof testing. However in each case the plate cracked (see Figure 60). In both cases fracture initiated from the outer edge of the plate. During combustion testing it is apparent that the outer edge of the plate is put into a tensile stress condition. Modifications are planned for this component. The outer diameter will be reduced and the thickness will be made more uniform.

The dilution band is made from isopressed sintered alpha silicon carbide. Four parts were received this period (see Figure 61). Table XII lists the NDE status for these parts.

Table XI. NDE and quality assessment for CBO flame holders.

FX No.	Visual	Penetrant	Quality	Comments
30483	OK	OK	A	In Mod I build
30484	OK	OK	A	
30485	Reject	Reject	C	Crack originated during forming or firing

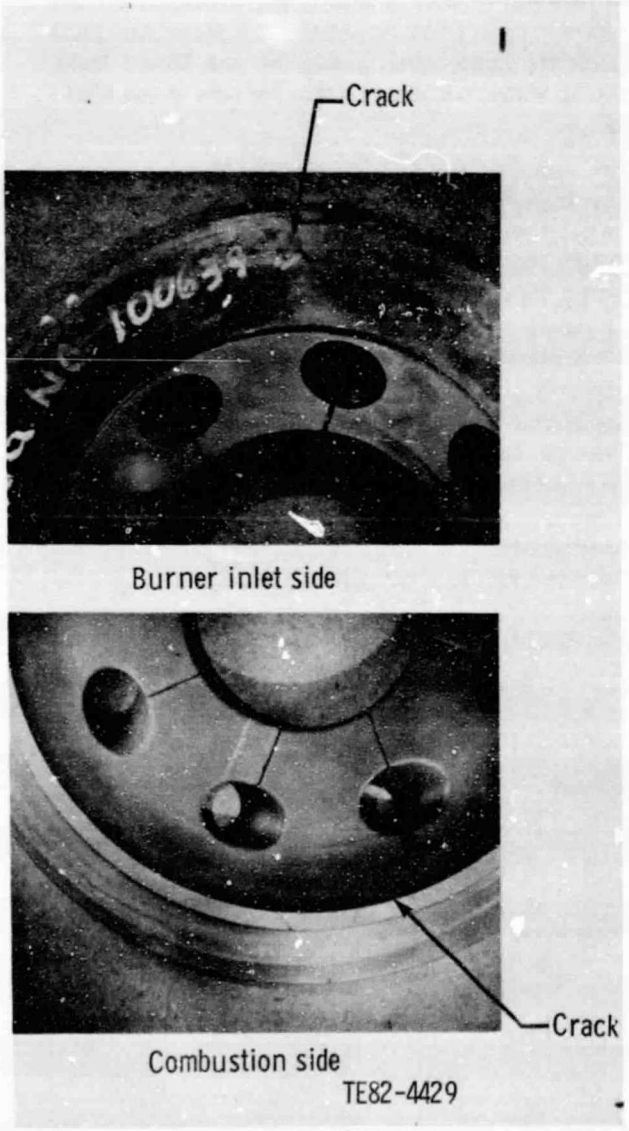

Figure 60. CBO swirl plate after burner rig testing.

Gasifier Scroll Assembly

The gasifier scroll assembly directs and contains the hot flowing gases into and through the gasifier rotor. Components that make up the assembly are the close-tolerance shroud, interconnecting duct, connecting adapter sleeve, and scroll shell. They will all be fabricated of sintered alpha silicon carbide.

The development effort centers on slip casting of the shell. Previous designs have not been adequate and are very difficult to slip cast. During this period a new mold was developed (see Figure 62) and scroll shells have been cast.

Figure 61. CBO dilution bands.

Table XII. NDE status for CBO dilution bands.

FX No.	Visual	Penetrant	X-ray	Comments
30433	OK	OK	OK	
30434	OK	OK	–	
30435	OK	OK	OK	In Mod I build
30436	OK	OK	OK	

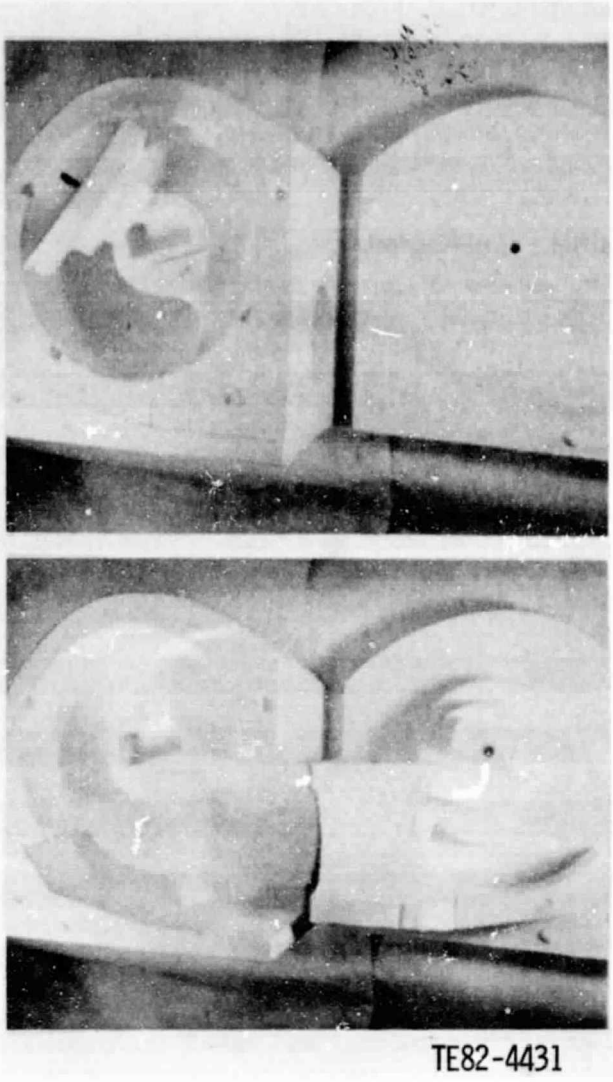

Figure 62. New gasifier scroll slip casting mold.

The interconnecting duct is produced from slip cast sintered alpha silicon carbide. After sintering it is machined to size. No problems have been encountered to date. A sintering fixture has been developed for support during initial firing.

The connecting adapter sleeve will be produced from green machined sintered alpha silicon carbide. Work has centered on finding the best grinding conditions to prevent cracking in the green state.

Close-tolerance shrouds will be produced from green-machined alpha silicon carbide. The vane pockets will be produced by ultrasonic machining in both the green and fired state. Figure 63 shows two green shrouds, and Figure 64 shows how the shroud will be positioned inside the scroll. The interconnecting duct will in turn fit into the smaller opening of the shroud. The individual components will be assembled by a sequence of sintering operations, then the interconnecting duct will be fired by itself. The a green adapter sleeve will be fixtured and fired so that it will be joined to the duct. The same operation will be performed for the close-tolerance shroud.

Scroll Backplates

The inner backplate is fabricated from sintered alpha silicon carbide by isopressing and green machining. Four parts have been produced this period. Limited NDE has not revealed any objectionable defects or surface indications.

Experiments were conducted to develop injection molding procedures for the outer backplate. CBO has reported that one backplate was fired free of any apparent flaws. Some dimensions were measured on two sintered backplates and are listed in Table XIII. The −1.55 mm (−0.061 in.) excess for dimension B indicates that there is a warpage problem. Work during the next period will involve further processing to alleviate the warpage and delivery of more outer backplates.

Power Turbine Vanes

These components are being produced with injection-molded sintered alpha silicon carbide. Forty-six have been received to date. Warping and distortion are still prevalent in these parts. However, there are enough parts of sufficient dimensional quality for the Mod I build. Figure 65 shows some vanes that are now in the Mod I build.

Zirconia Component Development

Low thermal conductivity zirconia components will play an important role in the operation of the present RPD AGT 100. Prototype zirconia components are being produced by the AC Spark Plug Division of General Motors and Kyocera International/Feldmulde.

AC Spark Plug is producing zirconia components by isopressing and green machining. Work to date has centered on characterization of this material.

Previous work has shown that the AC Spark Plug zirconia is very fine grained (smaller than 5 μm). Table XIV lists available property information for this material. This is a partially stabilized zirconia (PSZ) and possesses very uniform strength as a function of temperature.

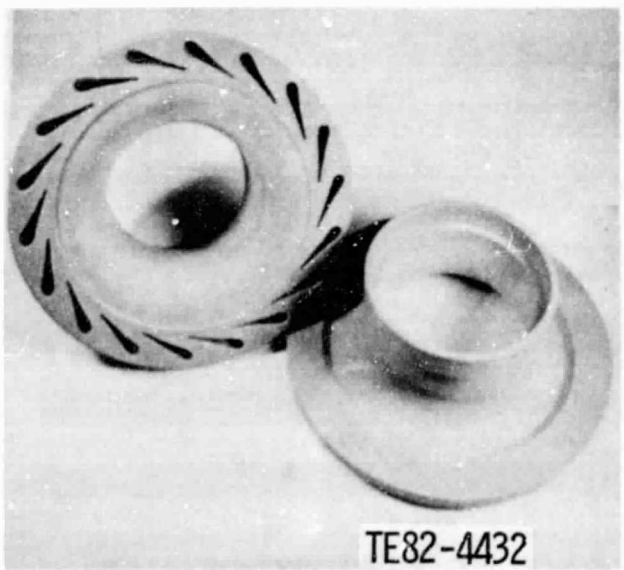

Figure 63. Close tolerance gasifier rotor shrouds.

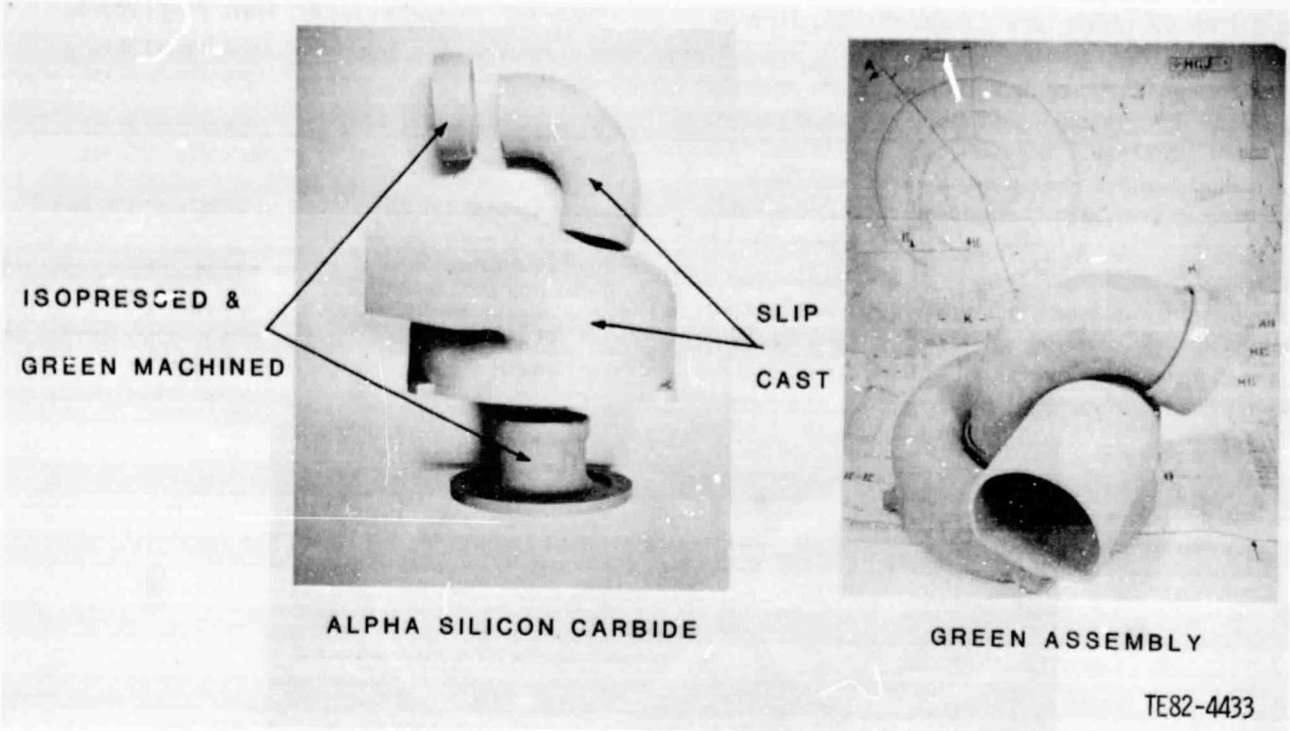

Figure 64. Gasifier scroll assembly.

Table XIII. Dimensional measurements for two sintered outer backplates.

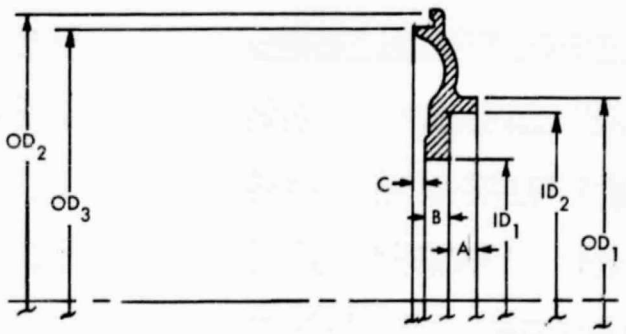

	Print—mm (in.)	Machining stock*—mm (in.) CBO No. 40-1	CBO No. 40-3
ID_1	113.55 (4.470)	0.38 (0.015)	0.64 (0.025)
ID_2	151.00 (5.945)	1.57 (0.062)	1.73 (0.068)
OD_1	163.00 (6.417)	−1.12 (−0.044)	−1.04 (−0.041)
OD_2	232.00 (9.134)	−0.13 (−0.005)	0.41 (0.016)
OD_3	220.01 (8.662)	−3.89 (−0.153	−2.97 (−0.117)
A	11.30 (0.445)	2.11 (0.083)	—
B	9.60 (0.378)	−1.55 (−0.061)	—
C	4.90 (0.193)	0.43 (0.017)	—
Density — g/cm^3		3.10	3.13

*Negative dimension indicates insufficient material for final machining.

Figure 65. Power turbine vanes.

Figure 66 shows some of the components received from Kyocera. Twelve parts for each component were received for appraisal. Of the 12 gasifier turbine retaining rings, 4 were defect free. Of the 12 shims, 8 were accept-

able. Of the 12 power turbine retainer rings, 10 were acceptable and defect free.

The material microstructure has been analyzed previously. This zirconia consists of a coarse-grained (~40 μm) cubic matrix, and within the large grains there are small monoclinic and tetragonal inclusions. The inclusions help to strengthen the material by inhibiting crack propagation. This is referred to as transformation toughened zirconia.

Room temperature strength qualification data for components received is as follows: MOR = 447.9 MPa (64.96 ksi), with a standard deviation of 31.0 MPa (4.49 ksi), for five machined surface test bars.

Table XIV. Properties for AC Spark Plug zirconia.

MOR at room temperature (machined)	343.3 MPa (49.79 ksi)
Standard deviation	22.9 MPa (12.72 ksi)
MOR at 1000°C (1832°F)	215.4 MPa (31.24 ksi)
Standard deviation	87.7 MPa (12.72 ksi)
Fracture toughness, K_{1c}	3.7 MPa·m$^{1/2}$ (1[illegible].0 ksi·in.$^{1/2}$)
Thermal expansion coefficient (Temprange: 40°C to 1000°C)	7.3·10^{-6}/°C
Thermal conductivity coefficient (25°C)	2.1 W/m °K
Specific gravity	5.72 g/cm^3

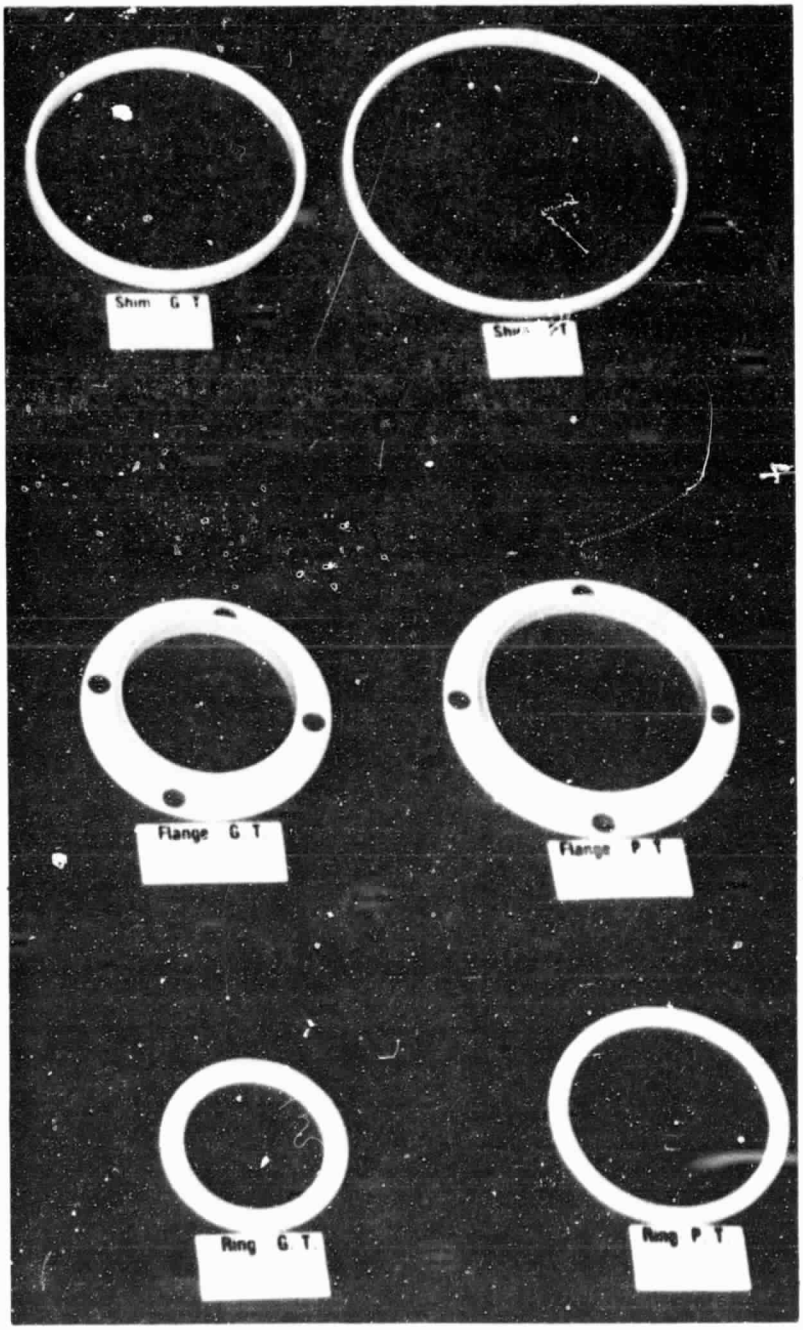

Figure 66. Zirconia components received from Kyocera.

X. Controls Development

The controls effort during this period has been to design and check out the electronic control system for the first scheduled dynamometer run. The electric control unit (ECU) to be used for this first test has been built using a modified digital control unit from another program.

An operator control console has been built and calibrated. This control console will allow manual open loop control of gasifier speed, inlet guide vanes, burner variable geometry, and power transfer clutch. It will also allow a ±111°C (±200°F) adjustment of the turbine outlet temperature limit and manual selection of fuel flow from the start nozzle to the main nozzle. Switches, lights, and meters are included to monitor the engine performance and to allow the control console operator to manipulate various engine conditions. Fuel flow is the only engine parameter that uses closed loop control, in which the amount of fuel flow is determined by the ECU software program and not manually set by an operator.

A test simulator has been built and is used to functionally check out the control system logic. All control console parameters are included. However, the actual control console can be connected to the simulator. Engine actuators, fuel system solenoids, thermocouples, and speed pickup signals are represented but only as a static checkout. That is, engine dynamics are not included. However, the simulator can be used as a valuable tool to check out the control software logic for shutdown faults, correct fuel valve current calculations, and ensure proper sequencing during starts/shutdowns.

The fuel system has been modified to provide higher pilot nozzle fuel flow for light-off and better fuel flow characteristics during start to main nozzle transition. These changes have been bench tested as a system to verify the desired performance. Component tests of the actuators and clutch valve have been completed. Engine hardware, such as inlet guide vanes and burner variable geometry, was tested with the actuators to verify actual movement and proper direction. A successful system checkout of the fuel system and the ECU was completed. Steady-state engine operating points were tested, using the test simulator, to check actual fuel flow to the engine as well as transient fuel flows when switching from start to main nozzle. Both tests show excellent correlation between predicted and actual fuel system performance.

The control software has been programmed into the ECU and was checked out using the test simulator. Numerous test points have been defined to check each control mode and the associated fuel valve current.

XII. Supportive Manufacturing, Cost, and Marketability

12.1 Manufacturing Feasibility—Pontiac Motor Division

Manufacturing feasibility studies at Pontiac have now been concluded on a majority of the engine components from detailed drawings. Manufacturing of these components is concentrated in two areas: (1) the Engine Component Machining and Assembly Manufacturing Engineering Department and (2) the Pressed Metal Manufacturing Engineering Department.

The manufacturing feasibility analysis from detailed drawings has been based on normal high-volume production processing and cost estimating procedures. During this analysis there has been extensive interaction and agreement between PMD Manufacturing and DDA Engineering regarding engine component design changes recommended to lower part cost, and design revisions proposed for compatibility with high-volume production machining and manufacturing requirements. This type of interaction will be reflected in the production RPD engine design.

Manufacturing Engineering has made proposals covering such areas as combining separate gears into cluster gear assemblies with resultant savings in machining and assembly operations; revisions to simplify various types of machining operations on separate gears, shafts, and pinions; revisions to the oil pump body, the regenerator housing, and the combustor assemblies; and several proposals on alternate materials to reduce cost. Manufacturing has also proposed that several shafts and gears be redesigned to a two-piece construction that allows utilization of a friction welding technique. A typical example, an output gear assembly, is shown in Figure 67. This pro-

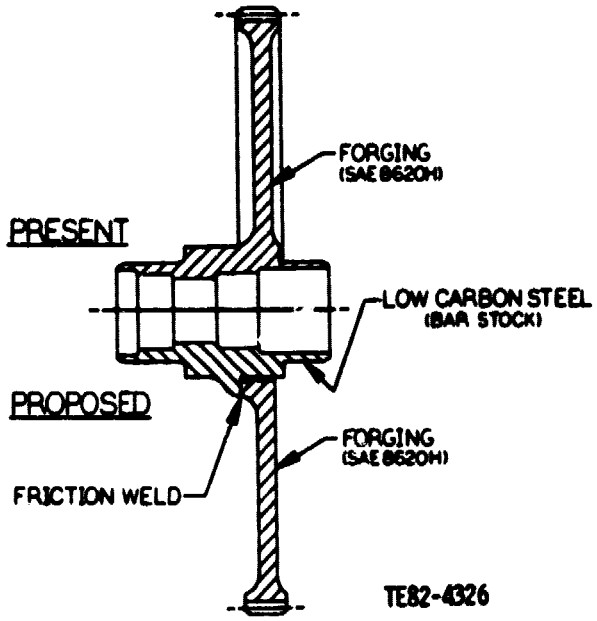

Figure 67. Output gear assembly.

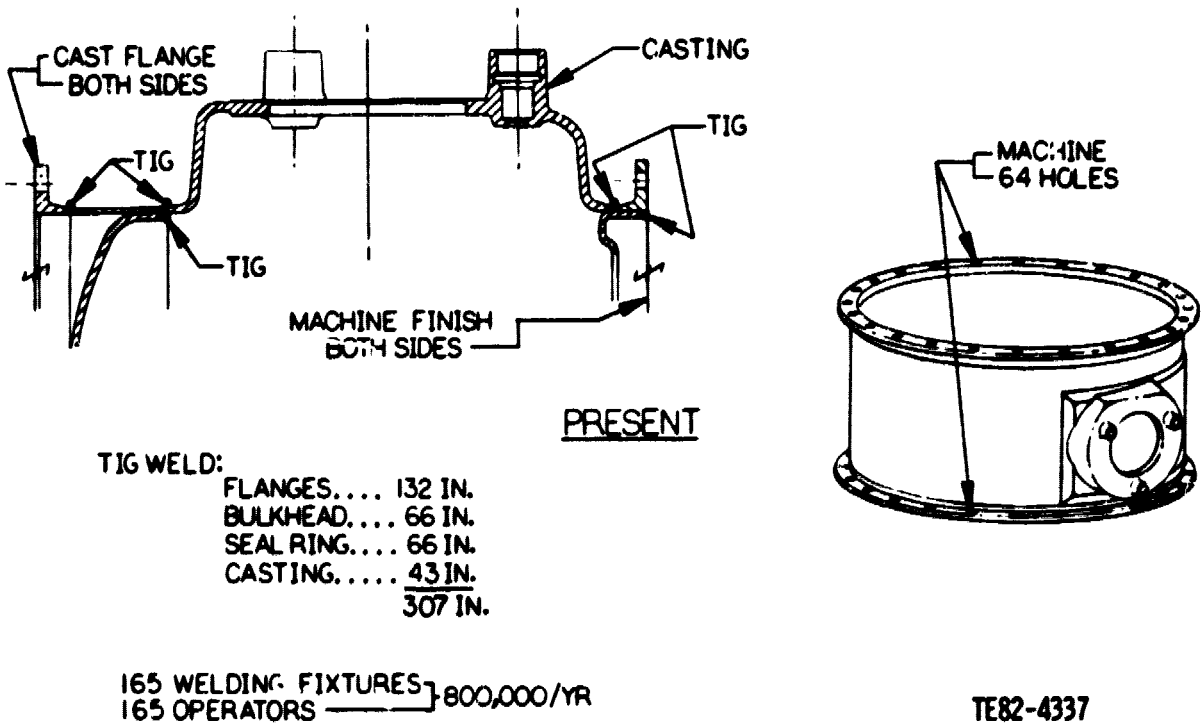

Figure 68. Present configuration of combustor case assembly.

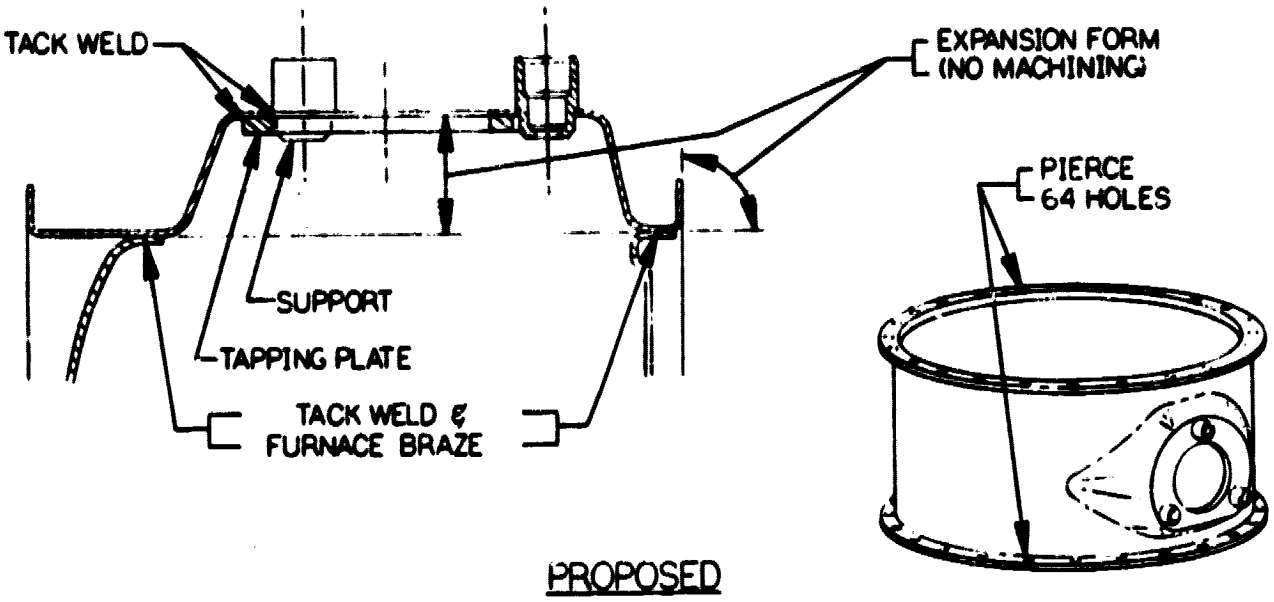

Figure 69. Proposed configuration of combustor case assembly.

posed construction yields a significant savings as a result of reducing the complexity and cost of the single gear forging by replacing the hub with a low-carbon steel part friction-welded to a simplified forging.

Manufacturing Engineering is continuing its investigation into state-of-the-art machining plus new processes applicable to manufacture of the engine. This includes such techniques as laser hole drilling and welding, electrical discharge machining, diamond wheel grinding, and balancing equipment and processing required to meet the critical balance requirements of the high-speed components. Additional work remains to be done on both manual and automated assembly techniques.

Pressed Metal Engineering has made proposals to DDA that have evolved from the department's formal processing studies on the major sheet metal components in the engine, such as the regenerator housing assembly, combustor case assembly, and several smaller parts. The major cost saving proposal has centered on redesign of the combustor case assembly. Figure 68 shows the original design, which consisted of a four-piece outer case: two cast flanges, the main body, and a cast combustor support. This design required extensive tungsten-inert-gas (TIG) welding to assemble the flanges and combustor support casting to the main body, and subsequent machining operations to qualify the flanges and drill the 64 holes required for engine assembly. Pressed Metal Engineering determined that the cost of this construction was prohibitive on a high-volume basis and proposed a redesign to DDA, which is shown in Figure 69. This redesign uses an expansion forming technique for both the combustor support area and the flanges. This process eliminates the TIG welding requirement and the machining required to qualify the flanges, and it also allows piercing of the 64 holes. In addition, the TIG welding of the inner bulkhead and seal ring is being replaced by furnace brazing, which occurs during heat treat, thus eliminating a specific welding operation. This proposal has resulted in a significant cost reduction. Figure 70 illustrates the significance of small savings at high volume

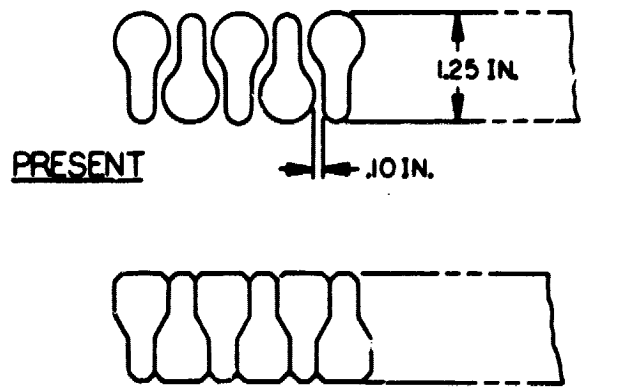

Figure 70. Inlet guide vane lever.

production levels. The inlet guide vane lever was originally designed such that 2.54 mm (0.10 in.) would be required between parts to maintain die steel life in a progressive die. A redesign was requested that allows the levers to be made with no waste material with a resultant savings of 19 miles of strip stock at 800,000 engines per year (15 levers per engine).

The Pressed Metal Engineering Department feels that similar significant gains can be made on the regenerator housing assembly, and the department will continue to pursue this and other cost reduction ideas when a die-development program is started in the future.

PMD Manufacturing, PMD Pressed Metal Engineering, and DDA Engineering feel that many other cost reductions will be achieved in the future through close manufacturing development/engine design interaction.

12.2 Cost Analysis— Pontiac Motor Division

The Industrial Engineering Department at Pontiac continues to develop a cost analysis of the engine based on the Manufacturing and Pressed Metal Engineering process routing cost estimates developed from detail drawings and from cost quotes received through Purchasing on components purchased from GM-Allied and outside suppliers. The following shows a sourcing analysis of the make and purchased parts in the engine assembly:

	Part No.
Make – Pontiac Motor Division	77
Purchase – GM-Allied Divisions	9
Purchase – Outside suppliers	284
Total part numbers	370

Appendix A. Terms and Definitions

Symbol/Term	Definition
AGT	advanced gas turbine
AGT 100	the AGT model being developed by DDA
AS	aluminum silicate
BIT	burner inlet temperature
BOT	burner outlet temperature
Btu	British thermal unit
BU	build number
BVG	burner variable geometry
C	isentropic spouting velocity $-2gJ\Delta h_{is}$
°C	degrees Celsius
CATE	a NASA/DOE development program "Ceramic Applications for Turbine Engines"
CBO	Carborundum Company
CDP	compressor discharge pressure
CGW	Corning Glass Works
CM	meridional chord
CO	carbon monoxide
corrected flow	flow $\sqrt{\Theta/\delta}$
CTE	coefficient thermal expansion
CY	calendar year
D_m	mean bearing diameter
DDA	Detroit Diesel Allison, Division of General Motors
DN	diameter of bore in mm x speed in rpm
DF-2	diesel fuel no. 2
DOE	US Department of Energy
ECU	electronic control unit
EDR	Engineering Development Report (of DDA)
equivalent flow	flow $\sqrt{\Theta_{cr}}/\delta$
equivalent speed	speed/ $\sqrt{\Theta_{cr}}$
equivalent work	$\Delta h/\Theta_{cr}$
°F	degrees Fahrenheit
ft	foot
g	gravitational constant
GM	General Motors Corporation
GPSIM	general purpose simulation
GTE	General Telephone and Electronics Corp.
green machining	machining a ceramic before it is fired
h	enthalpy
h or hr	hour
hp	horsepower
Hz	Hertz (frequency)
i.d.	inside diameter
IGV	inlet guide vane
in.	inch
J	conversion factor, Btu to ft-lb; Joule
JP-5	jet propulsion fuel no. 5
kg	kilogram
km	kilometer
ksi	thousand pounds per square inch
L	liter
LAS	lithium aluminum silicate
lbm	pound mass
LCF	low cycle fatigue
M	mega – (one million)
m	meter, Weibull modulus
M-dist	meridional distance
mm	millimeter
Mod I	the first design of AGT 100 using some ceramic hot section components
Mod II	the second AGT 100 design with ceramic hot section
MOR	modulus of rupture
N	force (Newton) or speed of rotation (rpm)
n	number of test samples
N1	gasifier speed of rotation
N2	power turbine speed of rotation
NASA	National Aeronautics and Space Administration
NDE	nondestructive evaluation
NO_x	oxides of nitrogen
o.d.	outside diameter
P	pressure
Pa	Pascal
PMD	Pontiac Motor Division of General Motors
psi	pounds per square inch
psig	pounds per square inch gage
PSZ	partially stabilized zirconia
Q	oil flow
°R	degrees Rankine
R_c	pressure ratio
R_e	turbine expansion ratio
RBSiC	reaction-bonded silicon carbide
RPD	reference power-train design
S	standard deviation
s or sec	second
SEM	scanning electron microscope
SLAM	scanning laser acoustic microscopy
S/N	serial number
SPAM	scanning photoacoustic spectroscopy
T	temperature
T_T	total temperature
T_{T_1}	total temperature, inlet
T/C	thermocouple
thixotropic casting	casting enhanced by vibration to reduce viscosity of the cast fluid
THM 440-T4	designation for a GM transmission for X-body cars
TOT	turbine outlet temperature
T-S	total-to-static

Symbol/Term	Definition
T-T	total-to-total
U_T	rotor tip speed
V	viscosity
VG	variable geometry
W	watt; bearing thrust load; mass flow
W_a	airflow
W_c	cooling flow rate
WOT	wide open throttle
2-D	two-dimensional (analysis)
3-D	three-dimensional (analysis)
404	an industrial gas turbine engine by DDA
505	an industrial gas turbine engine by DDA

Symbol/Term	Definition
γ	ratio of specific heats
Δ	difference between two measurements, e.g., ΔT
δ	pressure/pressure standard
Δh	specific work
Δh_{is}	ideal specific work (total-to-static)
ϵ	$(0.740/\gamma)\,(\gamma + 1/2)^{\gamma/\gamma - 1)}$
η	efficiency
θ	temperature/temperature standard
θ_{cr}	$(V_{cr}/V_{cr}std)^2$
$\bar{\sigma}$	average strength

1. Report No.	2. Government Accession No.	3. Recipient's Catalog No.
CR-168056		

4. Title and Subtitle	5. Report Date
ADVANCED GAS TURBINE (AGT) POWER-TRAIN SYSTEM FIFTH SEMIANNUAL	6. Performing Organization Code

7. Author(s)	8. Performing Organization Report No.
H. E. Helms, R. A. Johnson, R. K. Gibson, L. B. Smith	EDR 11185
	10. Work Unit No.

9. Performing Organization Name and Address	11. Contract or Grant No.
Detroit Diesel Allison, Division General Motors Corporation Box 894 Indianapolis, IN 46206	DEN 3-168
	13. Type of Report and Period Covered Contractor Report
12. Sponsoring Agency Name and Address U. S. Department of Energy Office of Vehicle and Engine Research Development Washington, DC 20545	14. Sponsoring Agency Code DOE/NASA

15. Supplementary Notes

Semiannual report. Prepared under Interagency Agreement DE-AI01-77CS51040. Project Manager P. T. Kerwin, Transportation Propulsion Division, NASA Lewis Research Center, Cleveland, OH 44135.

16. Abstract

Technical work on the design and effort leading to the testing of a 74.5 kW (100 hp) automotive gas turbine is described for the period January through June 1982. This is the fifth semiannual report. The general effort was concentrated on building an engine for test starting in July. The buildup progressed with only routine problems and the engine was delivered to the test stand 9 July. In addition to the engine build effort, work continued in selected component areas. Ceramic turbine parts were built and tested. Burst tests of ceramic rotors show strengths are approaching that achieved in test bars; proof testing is required for acceptable strength ceramic vanes. Over 25 hours was accumulated on the combustor rig in three test modes: pilot nozzle only, start nozzle, and main nozzle operation. Satisfactory ignition was achieved for a wide range of starting speeds and the lean blowout limit was as low as 0.06 kg/h (0.14 lb/hr). Lean blowout was more a function of nozzle atomization than fuel/air ratio. A variety of cycle points were tested. Transition from start nozzle flow to main nozzle flow was done manually without difficulty. The ceramic combustor assembly survived six days of testing without damage, but a crack developed in the ceramic combustor dome on the seventh day. A faulty preheater may have caused the failure. Regenerator parts were qualification tested without incident and the parts were assembled on schedule. Rig-based performance matched first build requirements. Repeated failures in the harmonic drive gearbox during rig testing resulted in that concept being abandoned for an alternate scheme. An extensive materials effort was continued by both DDA and the vendors. Thermal barrier development work showed advances in both mullite/cordierite and zircon-based systems. A large effort to characterize silicon carbide rotors showed that MOR strengths calculated from burst test results agreed with laboratory results from radial cut bars; values for axial cut bars were lower. Manufacturing and cost studies continued with the cooperation of Pontiac and generated several cost savings proposals.

17. Key Words (Suggested by Author(s))	18. Distribution Statement
Automotive gas turbine Ceramic components Alternate propulsion systems Improved fuel economy	Unclassified - unlimited

19. Security Classif. (of this report)	20. Security Classif. (of this page)	21. No. of Pages	22. Price*
Unclassified	Unclassified		

* For sale by the National Technical Information Service, Springfield, Virginia 22151